








Article

Crystal Structure, Vibrational, Spectroscopic and Thermochemical Properties of Double Sulfate Crystalline Hydrate $[\text{CsEu}(\text{H}_2\text{O})_3(\text{SO}_4)_2]\cdot\text{H}_2\text{O}$ and Its Thermal Dehydration Product $\text{CsEu}(\text{SO}_4)_2$

Yuriy G. Denisenko ¹, Maxim S. Molokeev ^{2,3,4}, Aleksandr S. Oreshonkov ^{5,6}, Alexander S. Krylov ⁵, Aleksandr S. Aleksandrovsky ^{7,8}, Nikita O. Azarapin ¹, Oleg V. Andreev ^{1,9}, Illaria A. Razumkova ¹ and Victor V. Atuchin ^{10,11,*}

¹ Department of Inorganic and Physical Chemistry, Tyumen State University, 625003 Tyumen, Russia; yu.g.denisenko@gmail.com (Y.G.D.); riddig@bk.ru (N.O.A.); o.v.andreev@utmn.ru (O.V.A.); razumkova@list.ru (I.A.R.)

² Laboratory of Crystal Physics, Federal Research Center KSC SB RAS, Kirensky Institute of Physics, 660036 Krasnoyarsk, Russia; msmolokeev@mail.ru

³ Institute of Engineering Physics and Radioelectronic, Siberian Federal University, 660041 Krasnoyarsk, Russia

⁴ Department of Physics, Far Eastern State Transport University, 680021 Khabarovsk, Russia

⁵ Laboratory of Molecular Spectroscopy, Federal Research Center KSC SB RAS, Kirensky Institute of Physics, 660036 Krasnoyarsk, Russia; oreshonkov@iph.krasn.ru (A.S.O.); shusy@iph.krasn.ru (A.S.K.)

⁶ School of Engineering and Construction, Siberian Federal University, 660041 Krasnoyarsk, Russia

⁷ Laboratory of Coherent Optics, Federal Research Center KSC SB RAS, Kirensky Institute of Physics, 660036 Krasnoyarsk, Russia; aleksandrovsky@kirensky.ru

⁸ Department of Photonics and Laser Technology, Siberian Federal University, 660041 Krasnoyarsk, Russia

⁹ Laboratory of Chemistry of Compounds of Rare-Earth Elements, Institute of Solid State Chemistry, UB RAS, 620137 Ekaterinburg, Russia

¹⁰ Laboratory of Optical Materials and Structures, Institute of Semiconductor Physics, SB RAS, 630090 Novosibirsk, Russia

¹¹ Research and Development Department, Kemerovo State University, 650000 Kemerovo, Russia

* Correspondence: atuchin@isp.nsc.ru; Tel.: +7-(383)-330-8889



Citation: Denisenko, Y.G.; Molokeev, M.S.; Oreshonkov, A.S.; Krylov, A.S.; Aleksandrovsky, A.S.; Azarapin, N.O.; Andreev, O.V.; Razumkova, I.A.; Atuchin, V.V. Crystal Structure, Vibrational, Spectroscopic and Thermochemical Properties of Double Sulfate Crystalline Hydrate $[\text{CsEu}(\text{H}_2\text{O})_3(\text{SO}_4)_2]\cdot\text{H}_2\text{O}$ and Its Thermal Dehydration Product $\text{CsEu}(\text{SO}_4)_2$. *Crystals* **2021**, *11*, 1027. <https://doi.org/10.3390/cryst11091027>

Academic Editor: Shujun Zhang

Received: 11 August 2021

Accepted: 23 August 2021

Published: 26 August 2021

Publisher's Note: MDPI stays neutral with regard to jurisdictional claims in published maps and institutional affiliations.



Copyright: © 2021 by the authors. Licensee MDPI, Basel, Switzerland. This article is an open access article distributed under the terms and conditions of the Creative Commons Attribution (CC BY) license (<https://creativecommons.org/licenses/by/4.0/>).

Abstract: Crystalline hydrate of double cesium europium sulfate $[\text{CsEu}(\text{H}_2\text{O})_3(\text{SO}_4)_2]\cdot\text{H}_2\text{O}$ was synthesized by the crystallization from an aqueous solution containing equimolar amounts of $1\text{Cs}^+ : 1\text{Eu}^{3+} : 2\text{SO}_4^{2-}$ ions. Anhydrous salt $\text{CsEu}(\text{SO}_4)_2$ was formed as a result of the thermal dehydration of the crystalhydrate. The unusual effects observed during the thermal dehydration were attributed to the specific coordination of water molecules in the $[\text{CsEu}(\text{H}_2\text{O})_3(\text{SO}_4)_2]\cdot\text{H}_2\text{O}$ structure. The crystal structure of $[\text{CsEu}(\text{H}_2\text{O})_3(\text{SO}_4)_2]\cdot\text{H}_2\text{O}$ was determined by a single crystal X-ray diffraction analysis, and the crystal structure of $\text{CsEu}(\text{SO}_4)_2$ was obtained by the Rietveld method. $[\text{CsEu}(\text{H}_2\text{O})_3(\text{SO}_4)_2]\cdot\text{H}_2\text{O}$ crystallizes in the monoclinic system, space group $P2_1/c$ ($a = 6.5574(1)$ Å, $b = 19.0733(3)$ Å, $c = 8.8364(2)$ Å, $\beta = 93.931(1)^\circ$, $V = 1102.58(3)$ Å³). The anhydrous sulfate $\text{CsEu}(\text{SO}_4)_2$ formed as a result of the thermal destruction crystallizes in the monoclinic system, space group $C2/c$ ($a = 14.327(1)$ Å, $b = 5.3838(4)$ Å, $c = 9.5104(6)$ Å, $\beta = 101.979(3)^\circ$, $V = 717.58(9)$ Å³). The vibration properties of the compounds are fully consistent with the structural models and are mainly determined by the deformation of non-rigid structural elements, such as H_2O and SO_4^{2-} . As shown by the diffused reflection spectra measurements and DFT calculations, the structural transformation from $[\text{CsEu}(\text{H}_2\text{O})_3(\text{SO}_4)_2]\cdot\text{H}_2\text{O}$ to $\text{CsEu}(\text{SO}_4)_2$ induced a significant band gap reduction. A noticeable difference of the luminescence spectra between cesium europium sulfate and cesium europium sulfate hydrate is detected and explained by the variation of the extent of local symmetry violation at the crystallographic sites occupied by Eu^{3+} ions, namely, by the increase in inversion asymmetry in $[\text{CsEu}(\text{H}_2\text{O})_3(\text{SO}_4)_2]\cdot\text{H}_2\text{O}$ and the increase in mirror asymmetry in $\text{CsEu}(\text{SO}_4)_2$. The chemical shift of the $^5\text{D}_0$ energy level in cesium europium sulfate hydrate, with respect to cesium europium sulfate, is associated with the presence of H_2O molecules in the vicinity of Eu^{3+} ion.

Keywords: sulfate; dehydration; crystal structure; Raman; thermal stability; photoluminescence

1. Introduction

The unusual electron configuration of rare-earth elements (REE) results in the specific chemical and physical properties of their compounds widely applied in glass and ceramic industries [1–10], nuclear engineering [11–13], electronic and photonic systems [14–26]. The 4*f* electrons of rare-earth elements are completely shielded by the filled 5*s* and 5*p* shells. The screening effect leads to the fact that the binding field only slightly affects the electrons of the 4*f* shell and it leads to the appearance of narrow absorption bands in the electronic spectra [7,27–30]. Unpaired *f* electrons determine not only the valence characteristics of rare-earth elements and spectroscopic parameters of their compounds, but also magnetic properties. Accordingly, in many REE compounds, paramagnetic and ferromagnetic effects were observed [31–36].

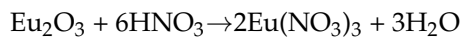
Among the REE elements, europium compounds are of particular interest, since Eu^{3+} ions provide efficient photoluminescence in the red spectral range highly needed for creating white LEDs with similar to daylight emission characteristics [37–46]. In recent years, a large number of studies related to the synthesis and properties of crystal phosphors doped with Eu^{3+} ions have appeared. However, in such systems, the doping level is usually very low and, often, the distribution of Eu^{3+} ions in the corresponding crystallographic positions is not obvious. For this reason, in complex compounds, it is difficult to clearly determine the relation between the coordination and spectroscopic parameters of Eu^{3+} ions in the host lattice. In such a situation, the compounds with a stoichiometric content of europium ions have attracted the increasing attention of researchers [37,38,47–53]. Self-activated phosphors are characterized by an almost complete absence of structural defects, and the precise determination of the crystal structure makes it possible to evaluate the relations between the Eu^{3+} ion coordination in the lattice and spectroscopic characteristics of the compound. Simple europium stoichiometric compounds with tetrahedral MO_4 units, where $M = \text{Mo}, \text{W}$ and S , were thoroughly studied and their applicability as highly efficient polyfunctional materials was shown [54–67]. At the same time, the properties of complex compounds of monovalent cations and rare-earth elements with tetrahedral anions are presented quite sporadically in the literature [37,48–51,53,68–72]. The structures and some properties of several double molybdates and tungstates with general composition $\text{AEu}(\text{MO}_4)_2$ ($A = \text{Li}, \text{Na}, \text{K}, \text{Cs}, \text{Rb}, \text{Ag}^+$; $M = \text{Mo}, \text{W}$) were investigated in the past and the examples of such contributions can be found elsewhere [72–76]. Contrary to that, the characterizations of the complex sulfate compounds of europium and monovalent cations are very scarce in the literature [53,68,69,71,77–81]. The present study is aimed at the observation of structural, thermal and spectroscopic characteristics of $[\text{CsEu}(\text{H}_2\text{O})_3(\text{SO}_4)_2] \cdot \text{H}_2\text{O}$ and $\text{CsEu}(\text{SO}_4)_2$. To the best of our knowledge, these sulfates have not been considered up to now. However, a structural similarity can be assumed between $[\text{CsEu}(\text{H}_2\text{O})_3(\text{SO}_4)_2] \cdot \text{H}_2\text{O}$ and earlier reported sulphate tetrahydrates $\text{ALn}(\text{SO}_4)_2 \cdot 4\text{H}_2\text{O}$ ($A = \text{Rb}, \text{Cs}, \text{Tl}, \text{NH}_4$) because of the similarity in the ionic radii of Cs^+ and these A^+ ions [69,80–86].

2. Methods and Materials

In the synthesis, the solutions of CsNO_3 , $\text{Eu}(\text{NO}_3)_3$ and H_2SO_4 were used as starting materials. For the solution preparation, twice distilled deionized water was used. The volumes of liquids were measured using glass pipettes and cylinders with the accuracy of 0.1 mL. Solid reagents were weighed on an analytical balance with the accuracy of 0.1 mg.

An europium nitrate solution was prepared using Eu_2O_3 (99.995%, TDM-96 Ltd., Russia). To remove carbonate and europium hydroxide impurities occasionally formed during their storage, the commodity oxide was calcined at 900 °C for 12 h, after which it was cooled to room temperature in a desiccator over silica gel. Subsequently, the calcined europium oxide, mass: 17.5963 g was transferred into a flask, and 21.6 mL of

concentrated nitric acid ($C(\text{HNO}_3) = 14.6 \text{ mol/L}$, $\rho = 1.3956 \text{ g/cm}^3$, ultrapure, Vekton Ltd., Nizhegorodsky, Russia) was added in small portions to the europium oxide. The mixture was carefully stirred until the oxide was completely dissolved according to equation:



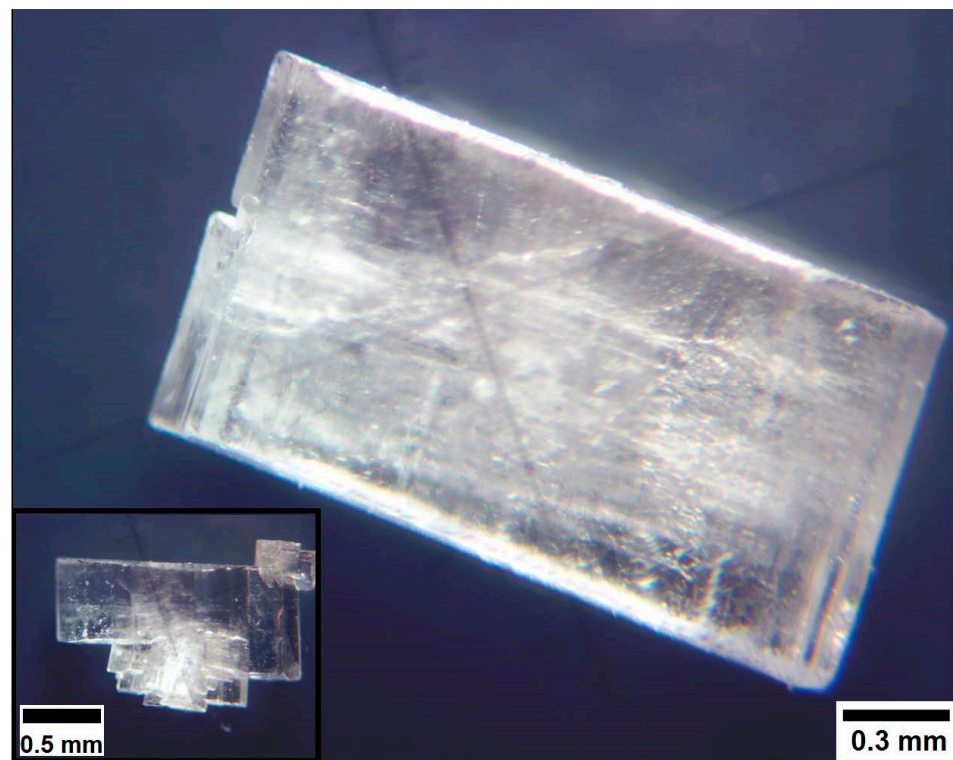
After the dissolution, the solution volume in the flask was adjusted to the mark with deionized water and mixed well for homogeneity. A sulfuric acid solution with the molar concentration of 2 mol/L was prepared by diluting concentrated sulfuric acid. To make this, 50 mL of water was poured into a 100.00 mL volumetric flask, then 11.17 mL of concentrated sulfuric acid ($C(\text{H}_2\text{SO}_4) = 17.9 \text{ mol/L}$, $\rho = 1.8349 \text{ g/cm}^3$, ultrapure, Vekton Ltd., Nizhegorodsky, Russia) was carefully poured in small portions, avoiding a strong heating of the solution. After this, the solution was naturally cooled to room temperature and the volume was adjusted to the mark with deionized water.

$[\text{CsEu}(\text{H}_2\text{O})_3(\text{SO}_4)_2] \cdot \text{H}_2\text{O}$ was obtained by a slow crystallization of the solution containing stoichiometric amounts of ions. For this, in a glass beaker, 10 mL of the CsNO_3 ($C(\text{Cs}^+) = 1 \text{ mol/L}$) solution, 10 mL of the $\text{Eu}(\text{NO}_3)_3$ ($C(\text{Eu}^{3+}) = 1 \text{ mol/L}$) solution and 10 mL of the H_2SO_4 ($C(\text{SO}_4^{2-}) = 2 \text{ mol/L}$) solution were mixed. The mixed solution was inserted into a desiccator over silica gel at 25 °C. In 12 h, the crystals precipitated from the mother liquor fell out in the reaction mixture. They were extracted, washed with ice water, pressed between filter paper sheets and dried in an empty desiccator to a constant weight. Anhydrous sulfate $\text{CsEu}(\text{SO}_4)_2$ was obtained by calcining the hydrate $[\text{CsEu}(\text{H}_2\text{O})_3(\text{SO}_4)_2] \cdot \text{H}_2\text{O}$ in a muffle furnace at the temperature of 500 °C for 10 h in the air. The $\text{CsEu}(\text{SO}_4)_2$ double sulfate was synthesized only in the powder form.

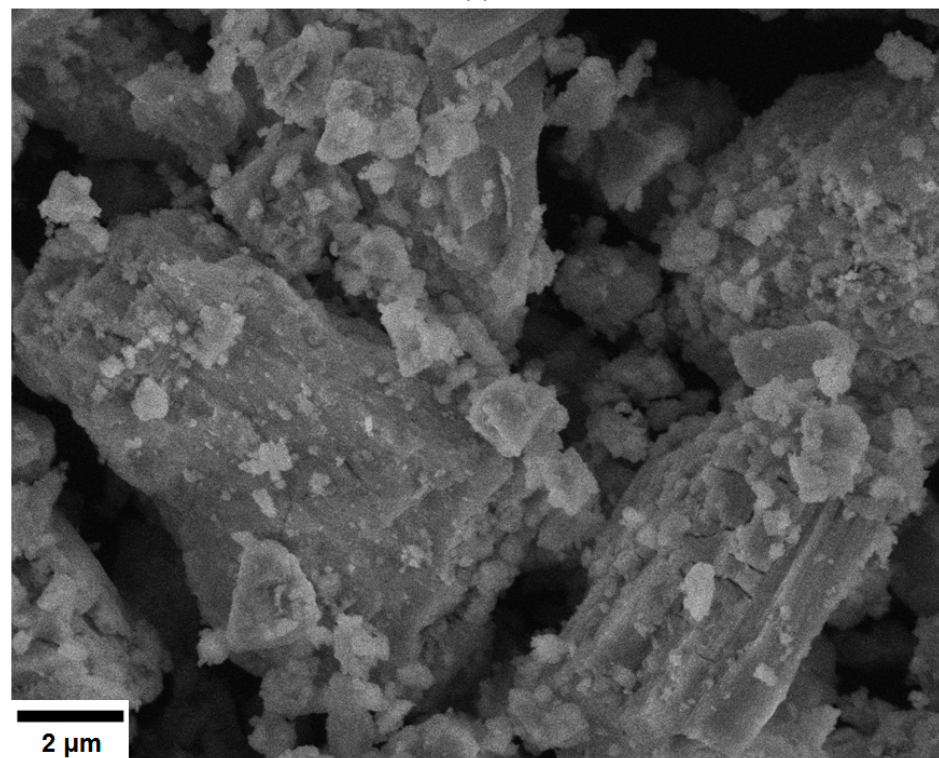
The photo images of the obtained single crystals of $[\text{CsEu}(\text{H}_2\text{O})_3(\text{SO}_4)_2] \cdot \text{H}_2\text{O}$, as observed with the use of optical microscope, are shown in Figure 1a. As it is seen, the crystals were transparent and they were well faceted, and that was a robust indicator of their high structural quality, as it was earlier observed for different materials [79,87–89]. The crystals were partly twinned due to the existence of several crystallization centers. The SEM pattern of $\text{CsEu}(\text{SO}_4)_2$ particles is given in Figure 1b. The product mainly contained loose aggregates. Such type of the particle micromorphology is commonly formed in powder compounds fabricated by the high-temperature decomposition process due to gas release effects [90,91].

The optical microscopy images of the crystals were fixed with an MS-2 microscope (State Optical Institute, Saint Petersburg, Russia) in reflected unpolarized light. The SEM patterns were exhibited using a JEOL JSM-6510LV scanning electron microscope. To avoid the surface charging effects, the powder samples were deposited on a conductive substrate (carbon tape) and covered with a nanometer gold layer (99.9%).

The single crystal X-ray diffraction data from $[\text{CsEu}(\text{H}_2\text{O})_3(\text{SO}_4)_2] \cdot \text{H}_2\text{O}$ were recorded by a SMART APEXII diffractometer (Mo K_α , $\lambda = 0.7106 \text{ \AA}$) at $T = 102(2) \text{ K}$. The orientation matrixes and cell parameters were calculated and refined by 45,124 reflections. The main information about the crystal data, data collection and refinement are reported in Table 1. The program APEXII (Bruker) was used to integrate the reflex intensities. Space group $P2_1/c$ was obtained by the analysis of extinction rules and intensity statistics obtained from all reflections. The multiscan absorption correction of reflection intensities was performed by the APEXII software (Bruker, 2003–2008, Karlsruhe, Germany). Then, the intensities of equivalent reflections were averaged. The structure was solved by the direct methods using package SHELXS and refined in the anisotropic approach for non-hydrogen atoms using the SHELXL program [92]. All hydrogen atoms of H_2O molecules were found via Fourier difference maps and, further, they were refined in a constrained mode. The structure test for the presence of other missing elements of symmetry and possible voids was produced using the PLATON program [93]. The DIAMOND program was used for the crystal structure plotting [94].



(a)



(b)

Figure 1. (a) Photo images of selected $[\text{CsEu}(\text{H}_2\text{O})_3(\text{SO}_4)_2] \cdot \text{H}_2\text{O}$ crystals and (b) an SEM pattern of the $\text{CsEu}(\text{SO}_4)_2$ powder.

Table 1. Main parameters of processing and Rietveld refinement of the $[\text{CsEu}(\text{H}_2\text{O})_3(\text{SO}_4)_2] \cdot \text{H}_2\text{O}$ and $\text{CsEu}(\text{SO}_4)_2$ powder samples.

Compound	$[\text{CsEu}(\text{H}_2\text{O})_3(\text{SO}_4)_2] \cdot \text{H}_2\text{O}$	$\text{CsEu}(\text{SO}_4)_2$
Space group	$P2_1/c$	$C2/c$
T, K	300 K	
a , Å	6.5574(1)	14.327 (1)
b , Å	19.0733(3)	5.3838 (4)
c , Å	8.8364(2)	9.5104 (6)
β , °	93.931(1)	101.979 (3)
V , Å ³	1102.58(3)	717.58 (9)
Z	4	4
R_{wp} , %	5.50	6.58
R_p , %	4.32	5.04
R_{exp} , %	2.93	3.00
χ^2	1.87	2.19
R_B , %	6.01	2.46

The powder diffraction data of $[\text{CsEu}(\text{H}_2\text{O})_3(\text{SO}_4)_2] \cdot \text{H}_2\text{O}$ and $\text{CsEu}(\text{SO}_4)_2$ for Rietveld analysis were collected at room temperature with a Bruker D8 ADVANCE powder diffractometer (Cu-K α radiation) and linear VANTEC detector. The step size of 2θ was 0.02° , and the counting time was 5 s per step. The Rietveld refinement was performed by using TOPAS 4.2 [95]. The structural parameters of $[\text{CsEu}(\text{H}_2\text{O})_3(\text{SO}_4)_2] \cdot \text{H}_2\text{O}$ determined by the single crystal analysis were used as a basis in powder pattern Rietveld refinement. For the $\text{CsEu}(\text{SO}_4)_2$ sample, all peaks were indexed by monoclinic cell ($C2/c$) with the parameters close to those of $\text{RbEu}(\text{SO}_4)_2$ [96]. Therefore, the crystal structure of $\text{RbEu}(\text{SO}_4)_2$ was taken as a starting model for Rietveld refinement, and, in the structure, the Rb ion was replaced by the Cs ion. The refinement was stable and gave low R-factors. The crystallographic data were deposited in Cambridge Crystallographic Data Centre (CSD# 2102324-2102325). The data can be downloaded from the site (www.ccdc.cam.ac.uk/data_request/cif) (accessed on 10 August 2021).

The Fourier-transformed infrared spectroscopy (FTIR) measurements were carried out with the use of a Fourier Transform Infrared Spectrometer FSM 1201 (Infraspek Ltd., Saint Petersburg, Russia). The sample for the investigation was prepared as a tablet with the addition of annealed KBr. The Raman spectra were recorded using an i-Raman Plus spectrometer (B&W Tek, Lubeck, Germany) at a laser excitation wavelength of 785 nm. The diffuse reflectance spectra were measured on a UV-2600 spectrophotometer (Shimadzu, Kyoto, Japan) equipped by the ISR-2600Plus attachment with an integrating sphere. The optical bandgap was estimated on the base of the measurements of diffuse reflectance spectra.

The calculation of electronic bandgap structures of $[\text{CsEu}(\text{H}_2\text{O})_3(\text{SO}_4)_2] \cdot \text{H}_2\text{O}$ and $\text{CsEu}(\text{SO}_4)_2$ was performed by using the DFT (density functional theory) method as implemented in the CASTEP code [97]. On-the-fly generated norm-conserving potentials were used and 5s5p6s, 4f5s5p6s, 3s3p, 2s2p and 1s electrons were treated as the valence ones for Cs, Eu, S, O and H, respectively. The self-consistent field tolerance was set to 2.0×10^{-7} eV/atom. The energy cutoff was chosen as 1143 eV for both compounds and superimposed by the $3 \times 1 \times 2$ k-point grid, in the case of $[\text{CsEu}(\text{H}_2\text{O})_3(\text{SO}_4)_2] \cdot \text{H}_2\text{O}$, and by the $4 \times 4 \times 2$ k-point grid in the case of $\text{CsEu}(\text{SO}_4)_2$. The local density approximation based on the Perdew and Zunger [98] parameterization of the numerical results of Ceperley and Alder [99] was used. The Hubbard U energy term $U_f = 6$ eV for the Eu 4f orbital was applied.

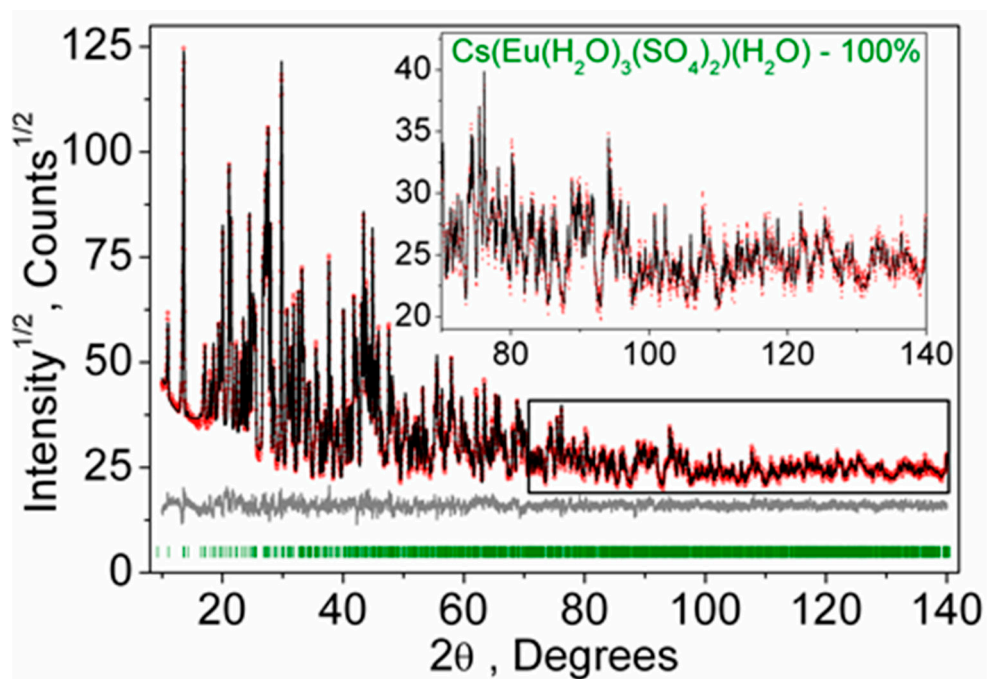
The thermal analysis was carried out in the argon flow with the use of a Simultaneous Thermal Analysis (STA) equipment 499 F5 Jupiter NETZSCH (NETZSCH Holding, Selb, Germany). The powder samples were inserted into alumina crucibles. The heating rate was 3 K/min. For the enthalpy determination, the equipment was initially calibrated with the use of standard metal substances, such as In, Sn, Bi, Zn, Al, Ag, Au, Ni. The heat effect peaks were determined with the package Proteus 6 2012.

The luminescence spectra under room temperature were registered on a HORIBA Jobin Yvon T64000 triple spectrometer with the spectral resolution 2.1 cm^{-1} using the excitation from the GaN laser at 410 nm and the power of 5 mW on the sample. The microscope based on Olympus BX-41 with the Olympus LMPlanFl 50 \times objective lens $f = 10.2 \text{ mm}$ with numerical aperture N.A. = 0.5 was used. The unfocused laser radiation illuminated the small sample powder quantity tangentially. The angle between incident laser light and the registered luminescence was about 60 degrees.

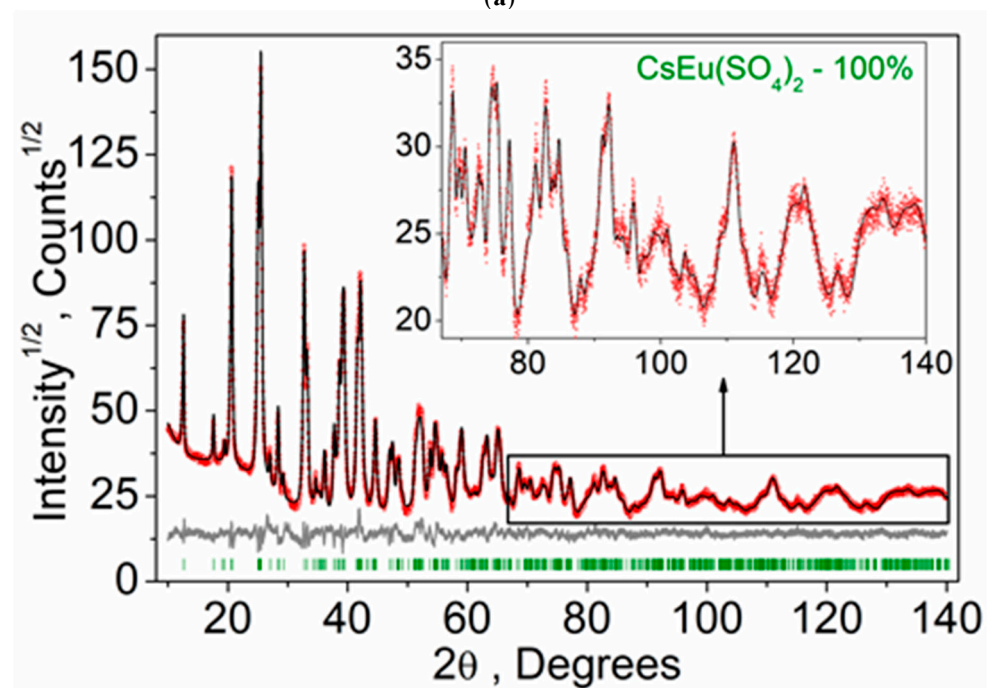
3. Results and Discussions

3.1. Crystal, Vibrational and Electronic Structure

According to the single crystal and powder diffraction analysis (Figure 2a, Tables 1 and S1–S5), $[\text{CsEu}(\text{H}_2\text{O})_3(\text{SO}_4)_2] \cdot \text{H}_2\text{O}$ crystallized in the monoclinic space group $P2_1/c$. The grown crystals did not contain any foreign crystalline impurity. The asymmetric part of the unit cell contained one Cs^+ ion, one Eu^{3+} ion, two S^{6+} ions, eight O^{2-} ions and four H_2O molecules. The Cs^+ ion in $[\text{CsEu}(\text{H}_2\text{O})_3(\text{SO}_4)_2] \cdot \text{H}_2\text{O}$ was coordinated by 13 O^{2-} ions forming a complex polyhedron. The Cs^+ ion was coordinated by four Eu ions, six SO_4 tetrahedra and two H_2O molecules. Each Eu^{3+} ion was coordinated by six O^{2-} ions and three H_2O molecules forming a $\text{EuO}_6(\text{H}_2\text{O})_3$ three-capped trigonal prism (Figure 3a). The $\text{EuO}_6(\text{H}_2\text{O})_3$ polyhedron was joined with two SO_4^{2-} tetrahedra by nodes and edges, respectively, forming, in total, a 2D net. The tridentate bridge–chelate μ_2 coordination of the anion towards Eu atoms was observed. One H_2O molecule was not coordinated to any metal and it should be considered as an isolated one. It was interesting to consider the stability of this type of structure in reference to the metal ion substitution. The collection of the known compounds $[\text{A}(\text{Ln}, \text{Ac})(\text{H}_2\text{O})_3(\text{SO}_4)_2] \cdot \text{H}_2\text{O}$ is presented in Table S6 (see Supplementary Materials) and the dependence of unit cell volume V_A on the ion radius IR of the Ln or Ac element is shown in Figure 4 [69,80–86]. It was evident that only such big-sized cations as $\text{A} = \text{NH}_4$, Tl, Rb and Cs provided a stable monoclinic structure. In this crystal family, the upper limit of $V_A = 1142.11 \text{ \AA}^3$ was reached in $[\text{CsLa}(\text{H}_2\text{O})_3(\text{SO}_4)_2] \cdot \text{H}_2\text{O}$, but the lower limit was unclear. At least, it was below or equal to $V_A = 1040.5 \text{ \AA}^3$ obtained in $[\text{RbEr}(\text{H}_2\text{O})_3(\text{SO}_4)_2] \cdot \text{H}_2\text{O}$. Up to now, the dominant part of the $[\text{A}(\text{Ln}, \text{Ac})(\text{H}_2\text{O})_3(\text{SO}_4)_2] \cdot \text{H}_2\text{O}$ crystals was synthesized for lanthanide elements and only three compounds were reported on for actinide elements. However, the monoclinic crystals $[\text{AAc}(\text{H}_2\text{O})_3(\text{SO}_4)_2] \cdot \text{H}_2\text{O}$ were reported on for all A cations, except for Cs, and it indicated that the search for new compounds among actinides is a promising field for future research activities. As seen in Figure 4, the $V_A(IR)$ dependences could be well approximated by the linear functions specific for each A element: $V_{\text{NH}_3} = 506.67 \text{ IR} + 433.28$, $V_{\text{Tl}} = 677.64 \cdot \text{IR} + 222.52$, $V_{\text{Rb}} = 438.36 \cdot \text{IR} + 515.74$ and $V_{\text{Cs}} = 420.25 \text{ IR} + 570.12$. These functions could be used for the prediction of unit cell volumes of other presently unknown crystals $[\text{ALn}(\text{H}_2\text{O})_3(\text{SO}_4)_2] \cdot \text{H}_2\text{O}$. For example, in $[\text{ALn}(\text{H}_2\text{O})_3(\text{SO}_4)_2] \cdot \text{H}_2\text{O}$, all possible V_{Cs} values should be in the range of $V_{\text{Cs}} = 1062.69 - 1142.11 \text{ \AA}^3$.



(a)



(b)

Figure 2. Difference Rietveld plots of (a) $[\text{CsEu}(\text{H}_2\text{O})_3(\text{SO}_4)_2] \cdot \text{H}_2\text{O}$ and (b) $\text{CsEu}(\text{SO}_4)_2$.

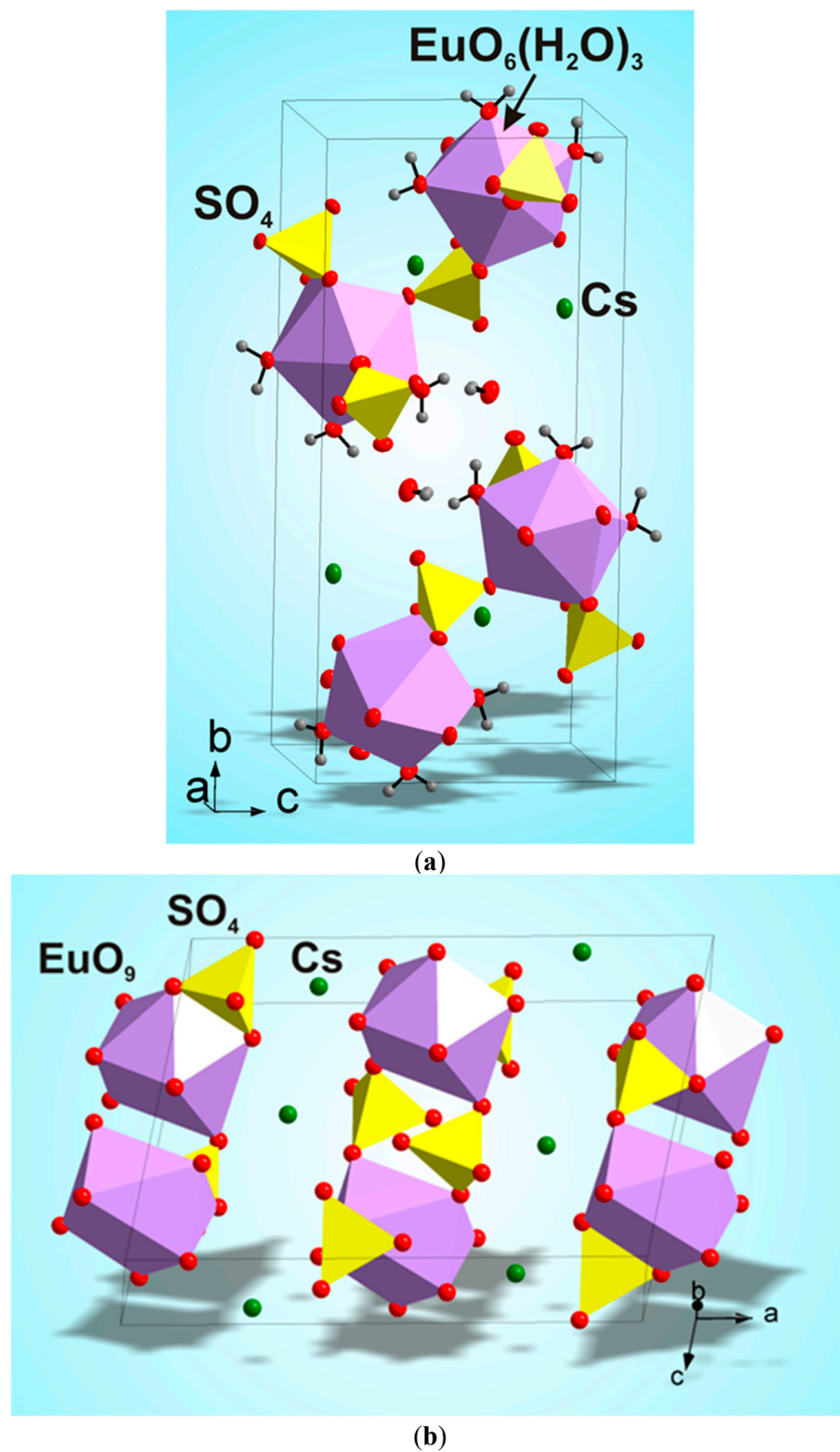


Figure 3. Crystal structures of (a) $[\text{CsEu}(\text{H}_2\text{O})_3(\text{SO}_4)_2] \cdot \text{H}_2\text{O}$ and (b) $\text{CsEu}(\text{SO}_4)_2$. The unit cells are outlined.

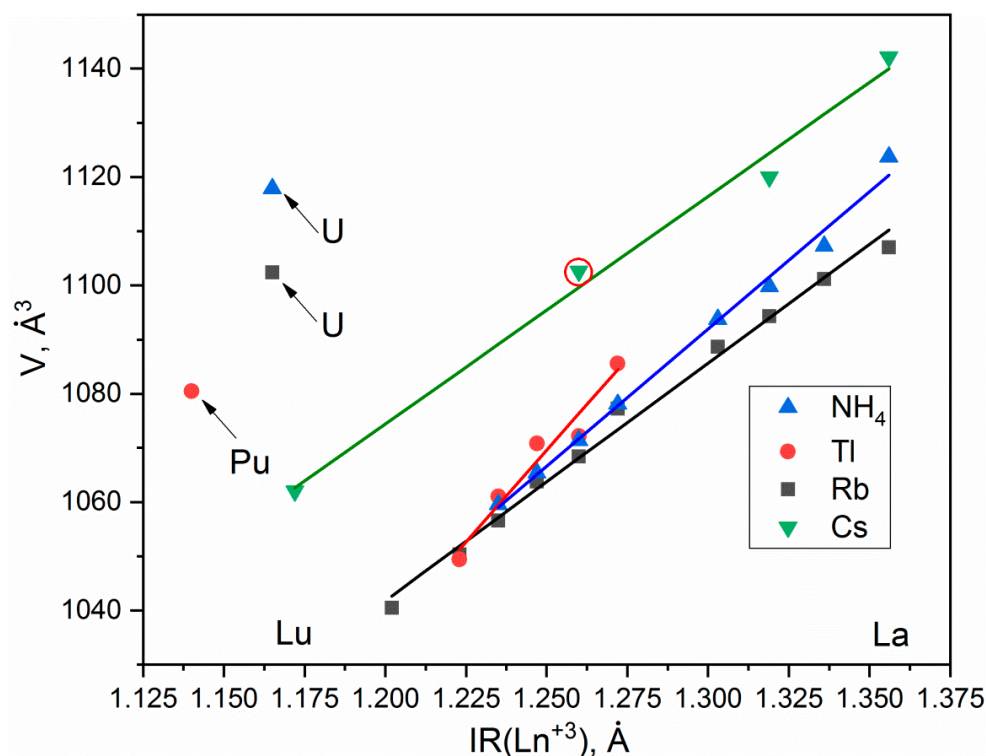


Figure 4. Unit cell volume dependences on the ionic radius of Ln^{3+} or Ac^{3+} ion for compounds $[\text{Cs}(\text{Ln},\text{Ac})(\text{H}_2\text{O})_3(\text{SO}_4)_2]\cdot\text{H}_2\text{O}$. The point of $[\text{CsEu}(\text{H}_2\text{O})_3(\text{SO}_4)_2]\cdot\text{H}_2\text{O}$ is highlighted by a red circle.

According to the results of the powder diffraction analysis (Figure 1b, Tables 1, S7 and S8), $\text{CsEu}(\text{SO}_4)_2$ crystallizes in the monoclinic space group $C2/c$. As it is seen in Figure 3b, the structure was of layered type. There were a half of Eu, a half of Cs ions and one SO_4 group in the asymmetric part of the unit cell. The Cs^+ ion in $\text{CsEu}(\text{SO}_4)_2$ was coordinated by 14 O^- ions forming a hexagonal dipyrmaid. In the $\text{CsEu}(\text{SO}_4)_2$ structure, the Cs^+ ion was coordinated by six Eu ions and eight SO_4 tetrahedra. Each Eu^{3+} ion was coordinated by six sulfate groups SO_4^{2-} via oxygen atoms. Two sulfate groups were chelately coordinated, while the rest were monodentate, resulting in the formation of a two-capped trigonal prism, and the coordination number of europium was equal to eight (Figure 3b). The tetradentate bridge–chelate μ_3 coordination mode of the anion towards Eu^{3+} was observed for $\text{CsEu}(\text{SO}_4)_2$. The structure of $\text{CsEu}(\text{SO}_4)_2$ was isostructural to that of $\text{RbEu}(\text{SO}_4)_2$ [96].

The vibrational spectra of $[\text{CsEu}(\text{H}_2\text{O})_3(\text{SO}_4)_2]\cdot\text{H}_2\text{O}$ and $\text{CsEu}(\text{SO}_4)_2$ are shown in Figure 5a,b, respectively. The normal vibrational modes of free $(\text{SO}_4)^{2-}$ ions had the wavenumbers of 450, 611, 983 and 1105 cm^{-1} for ν_2 , ν_4 , ν_1 and ν_3 vibrations, respectively [100]. The correlation for the internal vibrational modes of free sulfate ion and its site symmetry in the lattice and crystal symmetry for the investigated compounds are given in Table 2. Both sulfates had the same factor group symmetry and $(\text{SO}_4)^{2-}$ units occupied the identical symmetry sites. According to the structure refinement results, $\text{CsEu}(\text{SO}_4)_2$ was characterized by only one crystallographically independent SO_4 tetrahedron, while $[\text{CsEu}(\text{H}_2\text{O})_3(\text{SO}_4)_2]\cdot\text{H}_2\text{O}$ had two independent SO_4 units in its structure. Thus, the number of bands in the Raman and Infrared spectra in the regions of $(\text{SO}_4)^{2-}$ vibrations should have been twice as big in $[\text{CsEu}(\text{H}_2\text{O})_3(\text{SO}_4)_2]\cdot\text{H}_2\text{O}$ than in $\text{CsEu}(\text{SO}_4)_2$. This relation is clearly seen in Figure 6, where one strong band was found in the region of ν_1 symmetric stretching vibrations ($970\text{--}1100\text{ cm}^{-1}$) of SO_4 tetrahedra in the case of $\text{CsEu}(\text{SO}_4)_2$ and two bands in the case of $[\text{CsEu}(\text{H}_2\text{O})_3(\text{SO}_4)_2]\cdot\text{H}_2\text{O}$. The ν_3 vibrations were observed in the range of $1020\text{--}1250\text{ cm}^{-1}$. The ν_4 vibrational modes (antisymmetric bending) were located between 575 and 690 cm^{-1} . The ν_2 symmetric bending vibrations were found in the range of $400\text{--}520\text{ cm}^{-1}$. The strong multicomponent band of H_2O vibrations was observed in the Infrared spectrum of $[\text{CsEu}(\text{H}_2\text{O})_3(\text{SO}_4)_2]\cdot\text{H}_2\text{O}$, as seen in Figure 5a. The spectral bands

from 1550 to 1750 cm^{-1} were related to the H–O–H bending vibrations, while a wide band over 3000–3700 cm^{-1} appeared due to the symmetric O–H stretching. The total set of the Raman and Infrared modes observed in the experiment and their wavenumbers are presented in Table S9.

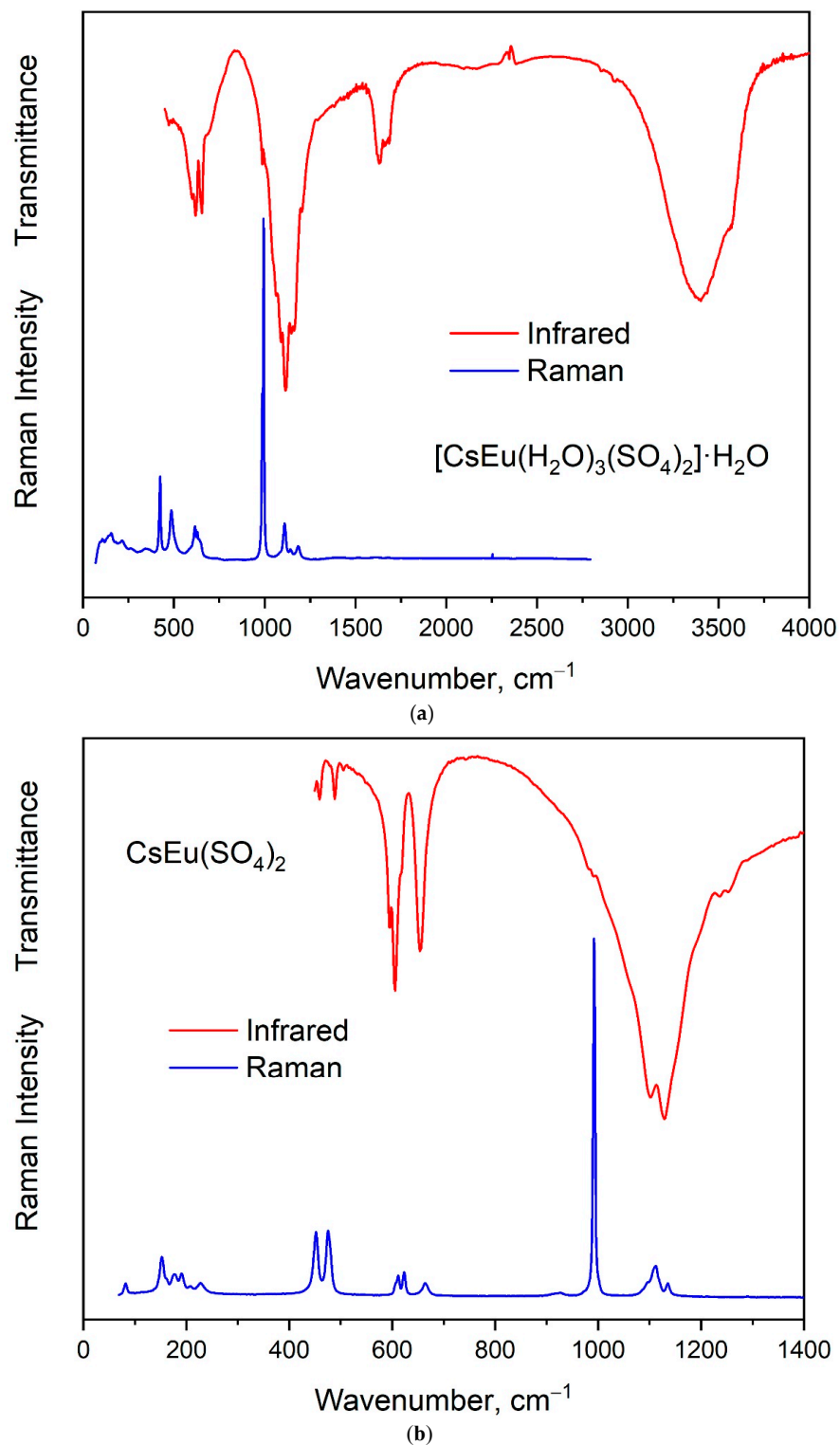
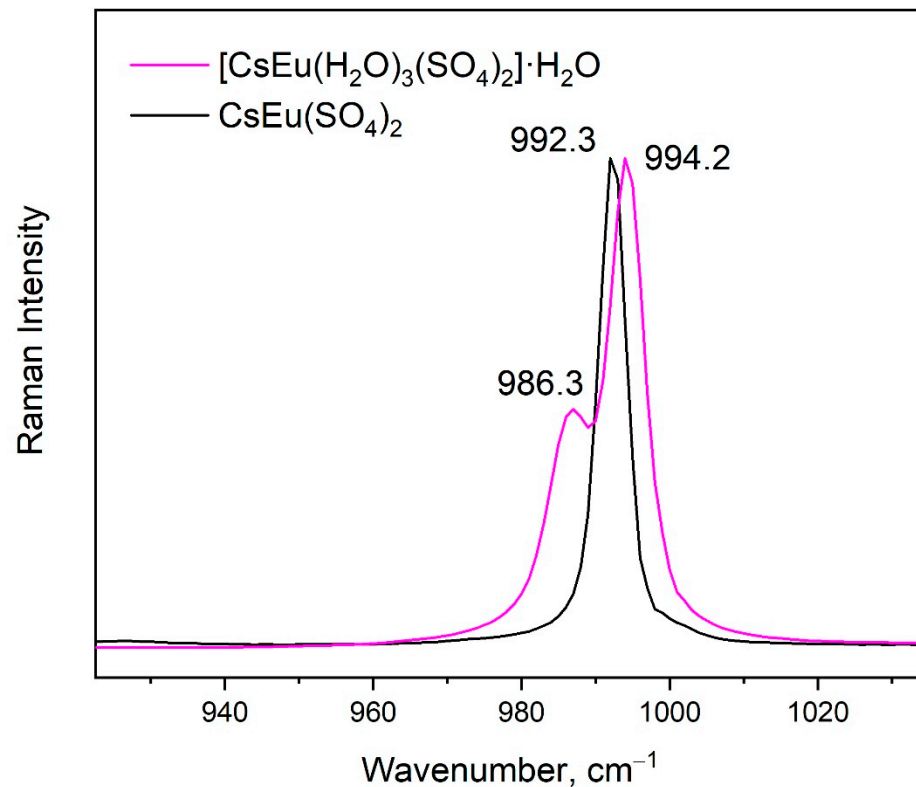


Figure 5. Infrared and Raman spectra of (a) $[\text{CsEu}(\text{H}_2\text{O})_3(\text{SO}_4)_2]\cdot\text{H}_2\text{O}$ and (b) $\text{CsEu}(\text{SO}_4)_2$.

Table 2. Correlation between molecular symmetry, site symmetry and factor group symmetry for SO_4^{2-} vibrations in $[\text{CsEu}(\text{H}_2\text{O})_3(\text{SO}_4)_2]\cdot\text{H}_2\text{O}$ and $\text{CsEu}(\text{SO}_4)_2$.

Molecular Symmetry T_d	Site Symmetry C_1	Group Symmetry C_{2h}
$A_1 (\nu_1)$	A	$A_g + A_u + B_g + B_u$
$E (\nu_2)$	$2A$	$2(A_g + A_u + B_g + B_u)$
$F_2 (\nu_3)$	$3A$	$3(A_g + A_u + B_g + B_u)$
$F_2 (\nu_4)$	$3A$	$3(A_g + A_u + B_g + B_u)$

**Figure 6.** Comparison of the Raman spectra of $[\text{CsEu}(\text{H}_2\text{O})_3(\text{SO}_4)_2]\cdot\text{H}_2\text{O}$ (purple curve) and $\text{CsEu}(\text{SO}_4)_2$ (black curve) in the range of sulfate tetrahedra stretching.

The band gap energies of $[\text{CsEu}(\text{H}_2\text{O})_3(\text{SO}_4)_2]\cdot\text{H}_2\text{O}$ and $\text{CsEu}(\text{SO}_4)_2$ were determined from the UV reflectance spectra with the use of the Kubelka–Munk function: $F(R) = K/S = (1 - R)/2R$, where K is the absorption coefficient, S is the scattering coefficient and R is the material reflectance. The Tauc plots [101], where the Kubelka–Munk function $(F(R)h\nu)^n$ was dependent on photon energy $h\nu$, are shown in Figure 7. The nature of electronic transition was determined by the exponent factor $n = 2$ or $1/2$ for direct or indirect electronic transitions, respectively. As it is seen in Figure 7a,b, the linear function extrapolation to the abscissa axis was successfully reached in the case of $n = 2$, and the direct band gap values were determined as those equal to 4.51 and 4.34 eV for $[\text{CsEu}(\text{H}_2\text{O})_3(\text{SO}_4)_2]\cdot\text{H}_2\text{O}$ and $\text{CsEu}(\text{SO}_4)_2$, respectively.

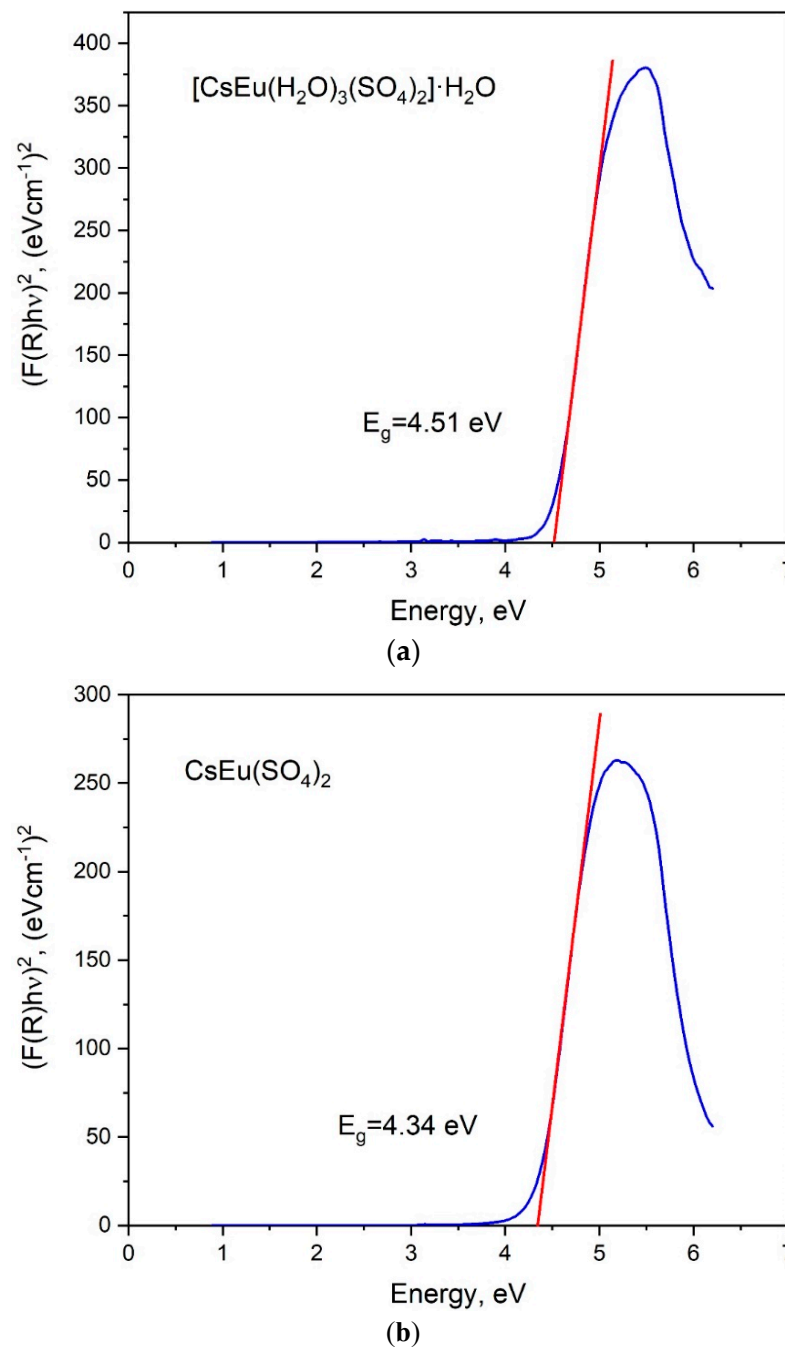


Figure 7. Tauc plots for (a) $[\text{CsEu}(\text{H}_2\text{O})_3(\text{SO}_4)_2] \cdot \text{H}_2\text{O}$ and (b) $\text{CsEu}(\text{SO}_4)_2$.

The paths along the Brillouin zone for the investigated compounds (Figure 8), chosen as a set of specific line segments connecting distinctive BZ points, should be written as: $\Gamma\text{-Z-D-B-}\Gamma\text{-A-E-Z-C}_2\text{-Y}_2\text{-}\Gamma$ for $[\text{CsEu}(\text{H}_2\text{O})_3(\text{SO}_4)_2] \cdot \text{H}_2\text{O}$ and $\Gamma\text{-C} \mid \text{C}_2\text{-Y}_2\text{-}\Gamma\text{-M}_2\text{-D} \mid \text{D}_2\text{-A-}\Gamma \mid \text{L}_2\text{-}\Gamma\text{-V}_2$ for $\text{CsEu}(\text{SO}_4)_2$ [102]. The coordinates of these points were: $\Gamma(0, 0, 0)$, $Z(0, 0.5, 0)$, $D(0, 0.5, 0.5)$, $B(0, 0, 0.5)$, $A(-0.5, 0, 0.5)$, $E(-0.5, 0.5, 0.5)$, $\text{C}_2(-0.5, 0.5, 0)$, $\text{Y}_2(-0.5, 0, 0)$ for $[\text{CsEu}(\text{H}_2\text{O})_3(\text{SO}_4)_2] \cdot \text{H}_2\text{O}$ (Figure 8a) and $\Gamma(0,0,0)$, $\text{C}(-0.287, 0.287, 0)$, $\text{C}_2(-0.713, -0.287, 0)$, $\text{Y}_2(-0.5, -0.5, 0)$, $\text{M}_2(-0.5, -0.5, 0.5)$, $\text{D}(-0.725, -0.275, 0.5)$, $\text{D}_2(-0.275, 0.275, 0.5)$, $\text{A}(0, 0, 0.5)$, $\text{L}_2(-0.5, 0, 0.5)$, $\text{V}_2(-0.5, 0, 0)$ for $\text{CsEu}(\text{SO}_4)_2$ (Figure 8b).

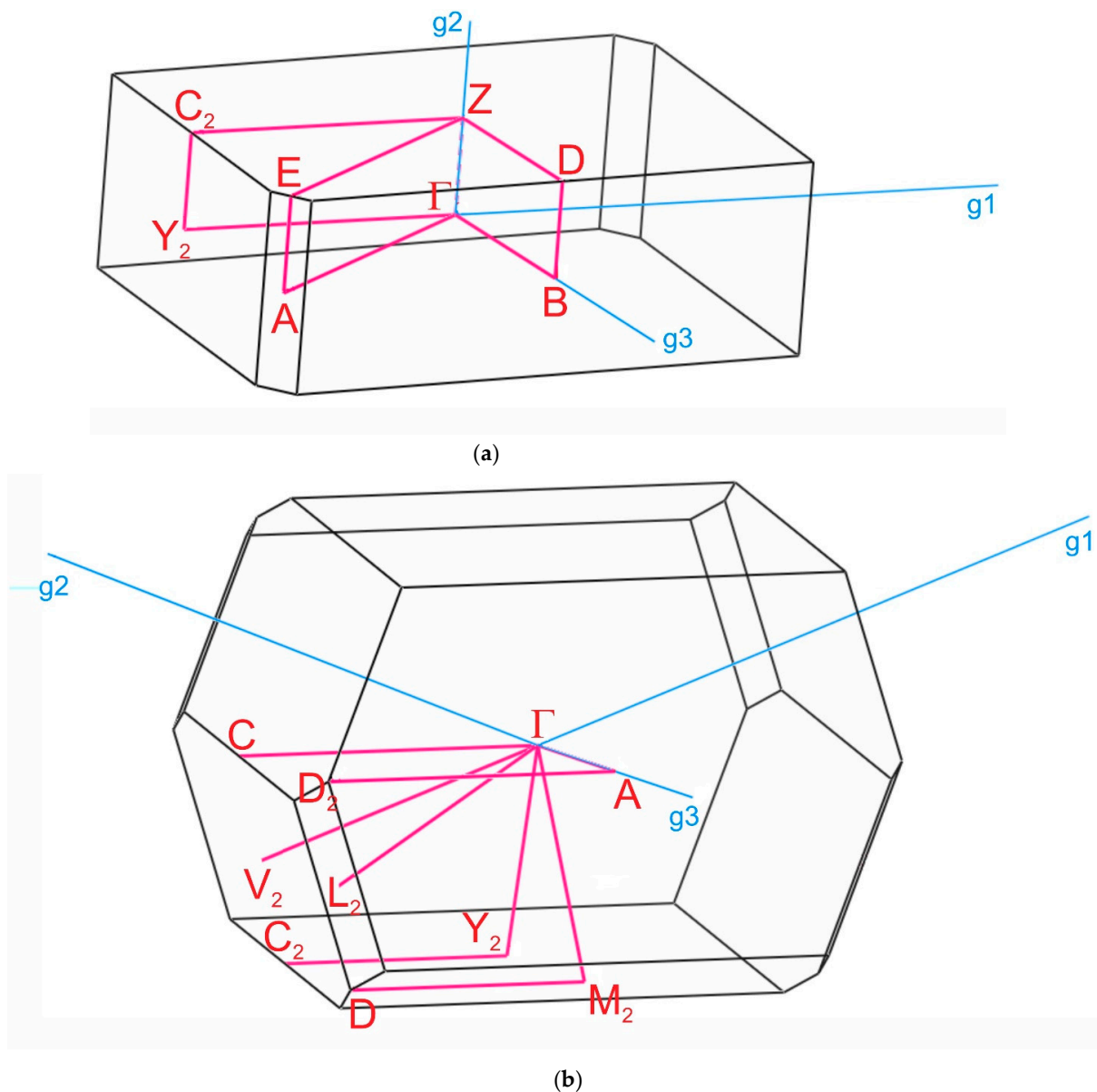


Figure 8. Brillouin zones of (a) $[\text{CsEu}(\text{H}_2\text{O})_3(\text{SO}_4)_2] \cdot \text{H}_2\text{O}$ and (b) $\text{CsEu}(\text{SO}_4)_2$.

The calculated electronic band structures of $[\text{CsEu}(\text{H}_2\text{O})_3(\text{SO}_4)_2] \cdot \text{H}_2\text{O}$ and $\text{CsEu}(\text{SO}_4)_2$ are shown in Figure 9. The bandgap calculated value was determined as the difference between the valence band top (VBT) and the conduction band bottom (CBB). As europium is a lanthanide, the band structure was presented as spin up and spin down components. The VBT and CBB points of $[\text{CsEu}(\text{H}_2\text{O})_3(\text{SO}_4)_2] \cdot \text{H}_2\text{O}$ and $\text{CsEu}(\text{SO}_4)_2$ were located in the center of the Brillouin zone (see Figure 9) and, thus, we can say that both compounds were direct band gap materials. The calculated bandgap value for $[\text{CsEu}(\text{H}_2\text{O})_3(\text{SO}_4)_2] \cdot \text{H}_2\text{O}$ was 5.09 eV, while, for $\text{CsEu}(\text{SO}_4)_2$, $E_g = 3.30$ eV. Thus, the transformation from the hydrate to the anhydrous compound reduced the bandgap value in the pair of sulfates.

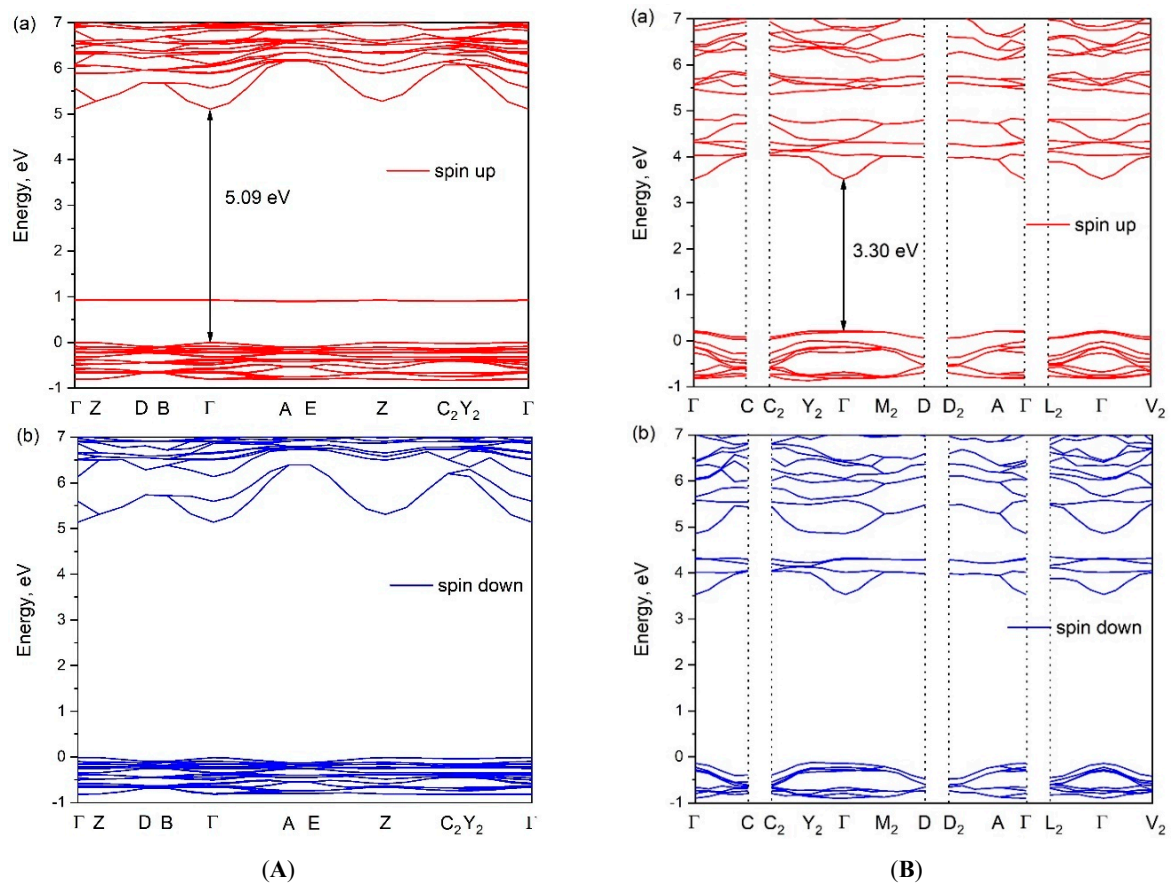


Figure 9. The electronic band structures of (A) $[\text{CsEu}(\text{H}_2\text{O})_3(\text{SO}_4)_2] \cdot \text{H}_2\text{O}$ and (B) $\text{CsEu}(\text{SO}_4)_2$.

The partial density of states (PDOS) for $[\text{CsEu}(\text{H}_2\text{O})_3(\text{SO}_4)_2] \cdot \text{H}_2\text{O}$ and $\text{CsEu}(\text{SO}_4)_2$ are shown in Figure 10 and the contribution of each type of atoms can be considered. It can be stated that the valence band top in both compounds was governed by the p electrons of oxygen, while the conduction band bottom was formed by the d electrons of Eu^{3+} ions. The small peak related to the f-electron state of Eu^{3+} ions appeared near the Fermi level in both cases.

3.2. Thermochemical Properties

Since anhydrous sulfate $\text{CsEu}(\text{SO}_4)_2$ was formed as a result of the $[\text{CsEu}(\text{H}_2\text{O})_3(\text{SO}_4)_2] \cdot \text{H}_2\text{O}$ dehydration, a full-scale study of thermochemical properties can be performed based only on the thermal analysis data shown for $[\text{CsEu}(\text{H}_2\text{O})_3(\text{SO}_4)_2] \cdot \text{H}_2\text{O}$ in a wide temperature range (Figure 11, Table 3). The $[\text{CsEu}(\text{H}_2\text{O})_3(\text{SO}_4)_2] \cdot \text{H}_2\text{O}$ dehydration proceeded in three stages and led to the formation of anhydrous sulfate $\text{CsEu}(\text{SO}_4)_2$. In the first stage, three water molecules were pinched off (effect A). The remaining water molecule was firmly bound in the structure and the dehydration process occurred in two stages, which corresponded to the formations of a hemihydrate (effect B) and anhydrous salt (effect C), respectively. Anhydrous sulfate $\text{CsEu}(\text{SO}_4)_2$ was stable up to 800 °C, and, at higher temperatures, a two-stage decomposition was observed. At the first stage (effect D), the decomposition into simple sulfates and decomposition of europium (III) sulfate occurred with the formation of europium oxysulfate $\text{Eu}_2\text{O}_2\text{SO}_4$. At the second stage (effect E), the europium oxysulfate decomposition took place. Thus, the final thermal destruction product at ~1200 °C was a mixture of cesium sulfate and europium oxide. This destruction mechanism resembled that of $\text{AgEu}(\text{SO}_4)_2$ [53], but, in the case of $\text{AgEu}(\text{SO}_4)_2$, the decomposition effects of the complex sulfate and those of europium sulfate were differentiated.

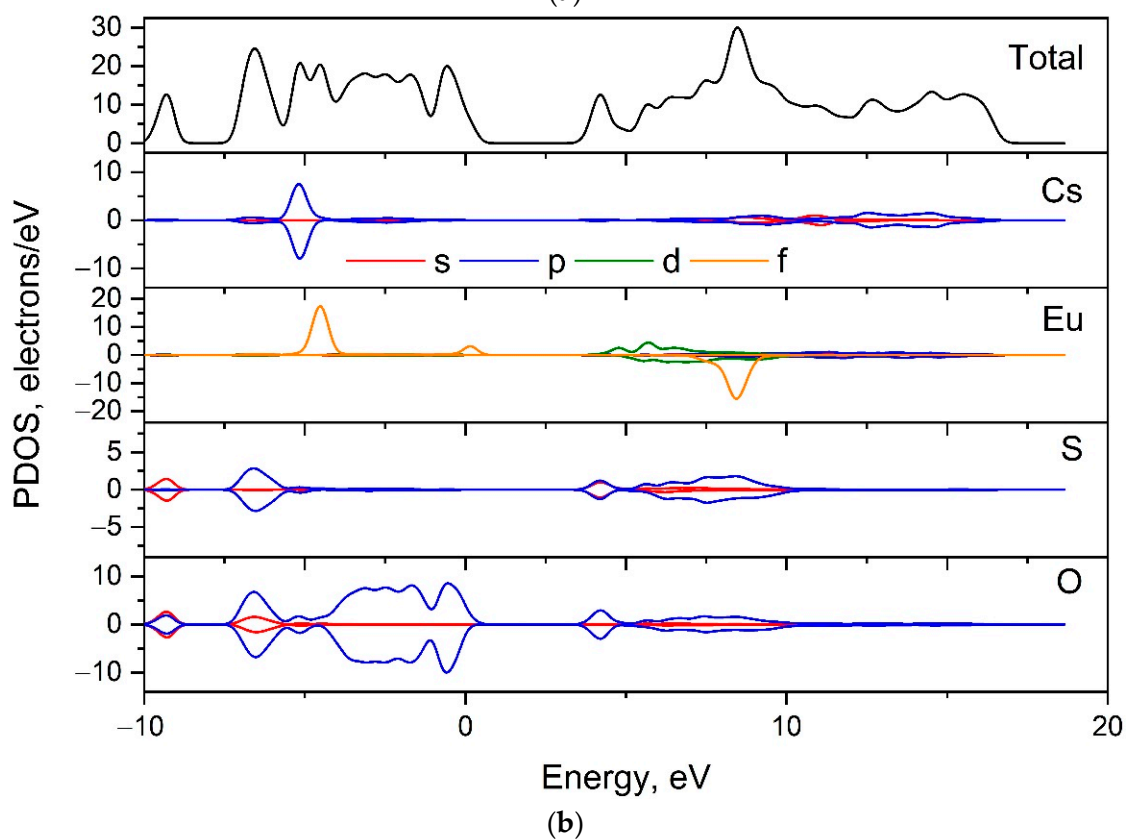
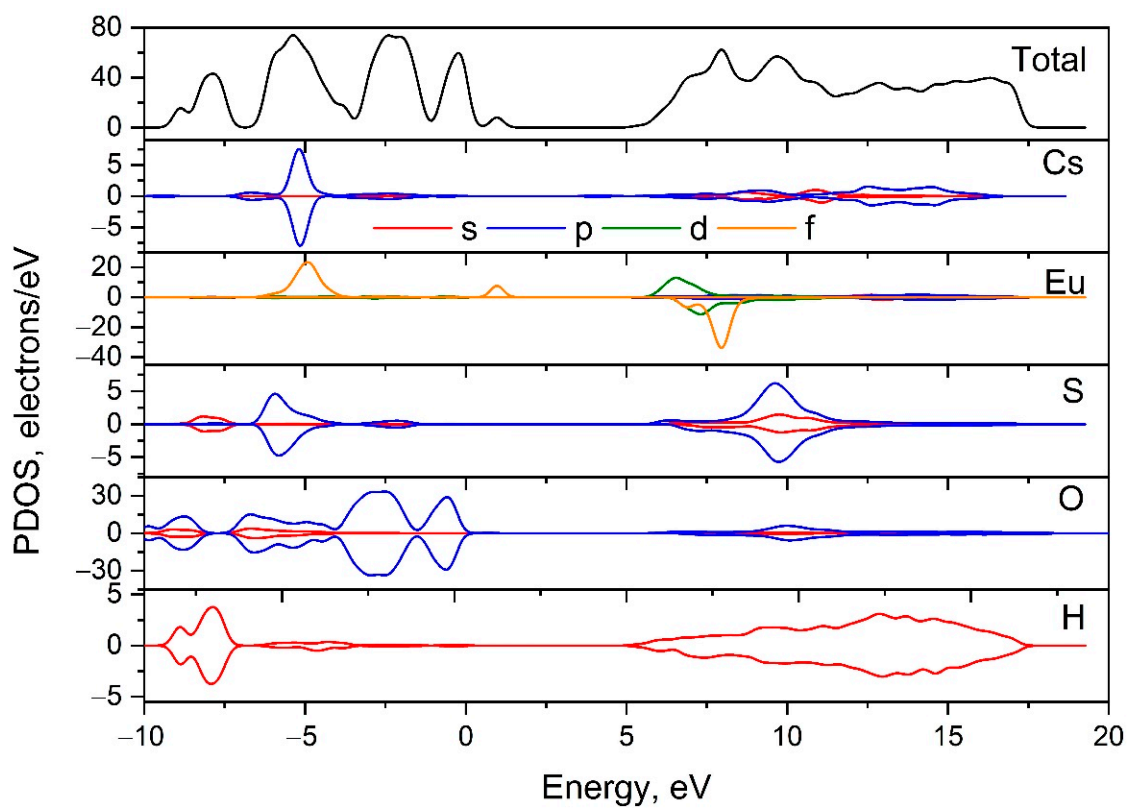


Figure 10. Electronic partial density of states in (a) $[\text{CsEu}(\text{H}_2\text{O})_3(\text{SO}_4)_2] \cdot \text{H}_2\text{O}$ and (b) $\text{CsEu}(\text{SO}_4)_2$.

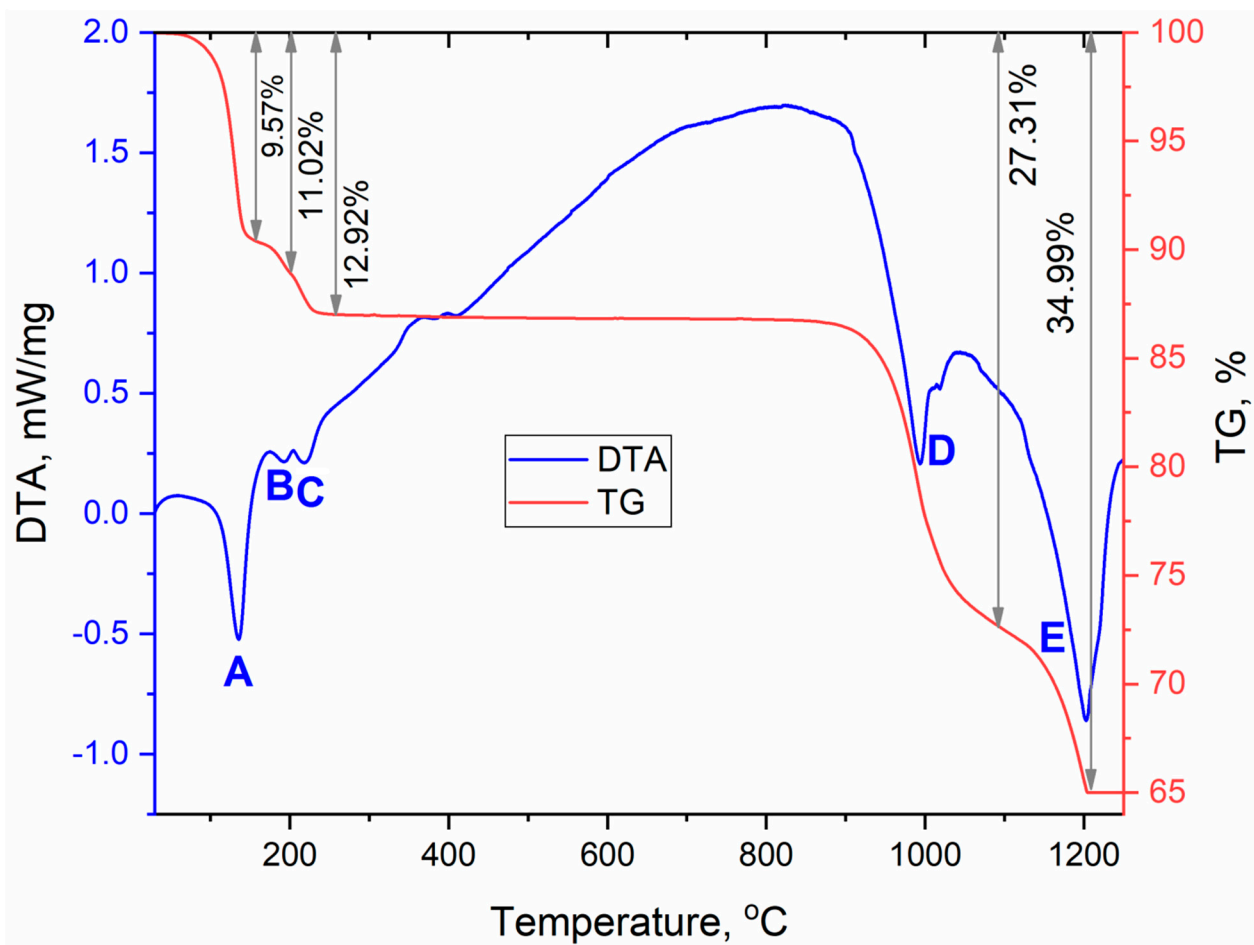


Figure 11. DSC/TG curves recorded for $[\text{CsEu}(\text{H}_2\text{O})_3(\text{SO}_4)_2]\cdot\text{H}_2\text{O}$.

Table 3. Thermal effects in $[\text{CsEu}(\text{H}_2\text{O})_3(\text{SO}_4)_2]\cdot\text{H}_2\text{O}$.

Effect	Reaction	References	Loss of Mass, %	
			Theoretical	Experimental
A	$[\text{CsEu}(\text{H}_2\text{O})_3(\text{SO}_4)_2]\cdot\text{H}_2\text{O} \rightarrow \text{CsEu}(\text{SO}_4)_2\cdot\text{H}_2\text{O} + 3\text{H}_2\text{O}\uparrow$	This work	9.85	9.57
B	$\text{CsEu}(\text{SO}_4)_2\cdot\text{H}_2\text{O} \rightarrow \text{CsEu}(\text{SO}_4)_2\cdot\frac{1}{2}\text{H}_2\text{O} + \frac{1}{2}\text{H}_2\text{O}\uparrow$		11.48	11.02
C	$\text{CsEu}(\text{SO}_4)_2\cdot\frac{1}{2}\text{H}_2\text{O} \rightarrow \text{CsEu}(\text{SO}_4)_2 + \frac{1}{2}\text{H}_2\text{O}\uparrow$		13.13	12.92
D	$\text{CsEu}(\text{SO}_4)_2 \rightarrow \text{Cs}_2\text{SO}_4 + \text{Eu}_2\text{O}_2\text{SO}_4 + 2\text{SO}_2 + \text{O}_2$	[48,67]	27.71	27.31
E	$\text{Eu}_2\text{O}_2\text{SO}_4 \rightarrow \text{Eu}_2\text{O}_3 + \text{SO}_2 + \frac{1}{2}\text{O}_2$		35.00	34.99

The most interesting feature of the $[\text{CsEu}(\text{H}_2\text{O})_3(\text{SO}_4)_2]\cdot\text{H}_2\text{O}$ dehydration process was the unusual water molecules evaporation order, which seemed to be impossible on the base of the crystal structure, where three water molecules were coordinated to the europium atom, and one water molecule was in the void of the crystal structure. Commonly, in solids under heating, water molecules in voids are lost first and, then, coordinated water molecules are evaporated. However, in $[\text{CsEu}(\text{H}_2\text{O})_3(\text{SO}_4)_2]\cdot\text{H}_2\text{O}$, the order was opposite. To explain this phenomenon, it is necessary to consider in detail the coordination of water molecules in the structure and the system of hydrogen bonds shown in Figure 12. It was obvious that the detachment of an uncoordinated water molecule would cause the destabilization of the molecules bound to the O10 and O15 atoms, and it determined the pinching off of these three H₂O molecules in one stage. At the same time, the water molecule bound to the O9 atom was very tightly coordinated by the europium polyhedron and two sulfate tetrahedra, and this fact determined its increased stability. It could be intriguing

to compare the thermal dehydration processes in $[\text{CsEu}(\text{H}_2\text{O})_3(\text{SO}_4)_2]\cdot\text{H}_2\text{O}$ and other isostructural compounds listed in Table S6. However, to our best knowledge, the results of the thermochemical analysis are available only for $[\text{Tl}(\text{Ln},\text{Ac})(\text{H}_2\text{O})_3(\text{SO}_4)_2]\cdot\text{H}_2\text{O}$ [69]. In $[\text{Tl}(\text{Ln},\text{Ac})(\text{H}_2\text{O})_3(\text{SO}_4)_2]\cdot\text{H}_2\text{O}$, three water molecules were evaporated first, and, at the second stage, the fourth water molecule was lost. Thus, the dehydration routes in $[\text{Tl}(\text{Ln},\text{Ac})(\text{H}_2\text{O})_3(\text{SO}_4)_2]\cdot\text{H}_2\text{O}$ and $[\text{CsEu}(\text{H}_2\text{O})_3(\text{SO}_4)_2]\cdot\text{H}_2\text{O}$ were different. Unfortunately, a detailed analysis of the different behavior of these crystals was impossible because only the cell parameters were reported for $[\text{Tl}(\text{Ln},\text{Ac})(\text{H}_2\text{O})_3(\text{SO}_4)_2]\cdot\text{H}_2\text{O}$ [69], and their crystal structures remain unknown.

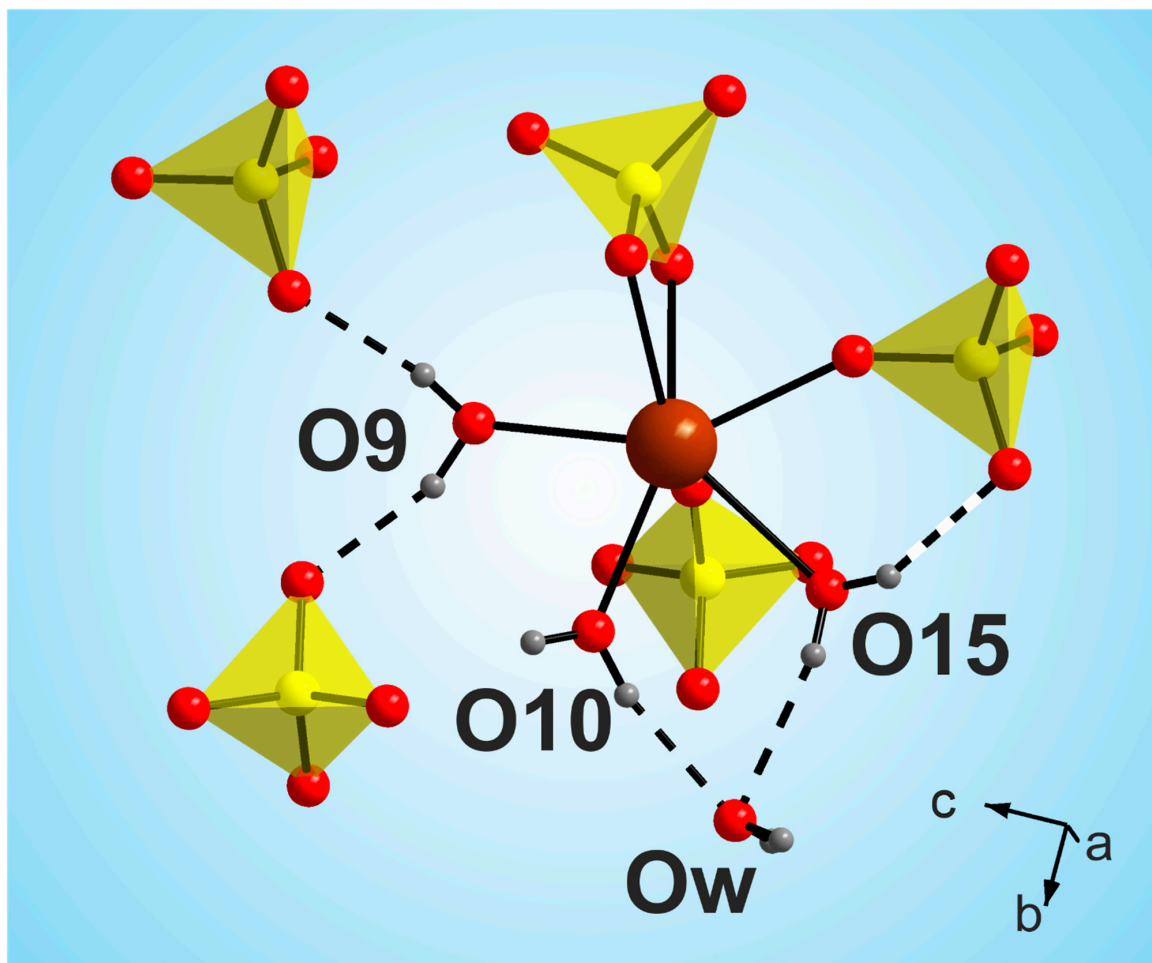


Figure 12. Coordination of water molecules in the $[\text{CsEu}(\text{H}_2\text{O})_3(\text{SO}_4)_2]\cdot\text{H}_2\text{O}$ structure.

3.3. Luminescence Properties

The exciting radiation at 410 nm used for luminescent measurements fell into the resonance with the transition from the ground state $^7\text{F}_0$ to the $^5\text{D}_3$ state of the Eu^{3+} ion. The luminescence from $^5\text{D}_3$, $^5\text{D}_2$ and $^5\text{D}_1$ states was negligible, as compared to that from the $^5\text{D}_0$ state. The spectra of luminescence from the $^5\text{D}_0$ state are presented in Figure 13 for both cesium europium sulfate and cesium europium sulfate hydrate. Both crystals belong to the monoclinic symmetry class but to different space groups ($\text{C}2/c$ and $\text{P}2_1/c$, correspondingly), and the luminescent spectra of the Eu^{3+} ion drastically differed. The local symmetry of the Eu^{3+} ion in cesium europium sulfate was C_2 , while in cesium europium sulfate hydrate it was C_1 . This difference seemed to be of minor importance; however, from the spectra, additional features of the local environment could be deduced. The amplitudes of luminescent bands at the magnetic dipole $^5\text{D}_0 \rightarrow ^7\text{F}_1$ transition and at the crystal-field-induced $^5\text{D}_0 \rightarrow ^7\text{F}_2$ transition were almost equal, and that indicated a relatively

low deviation from the inversion symmetry at the Eu^{3+} ion site in cesium europium sulfate (Figure 14a). Alternatively, the crystal-field-induced ${}^5\text{D}_0 \rightarrow {}^7\text{F}_2$ transition confidently dominated in cesium europium sulfate hydrate, indicating a much larger violation of the inversion symmetry at the Eu site in this hydrate crystal (Figure 14b). Using the Judd–Ofelt analysis (see, e.g., paper by Kolesnikov et al. [103]), the radiative lifetime of Eu ion in cesium europium sulfate hydrate was 2.27 times smaller than in cesium europium sulfate due to a larger violation of inversion symmetry specified above. At the same time, the ultranarrow line amplitude of at the ${}^5\text{D}_0 \rightarrow {}^7\text{F}_0$ transition in cesium europium sulfate was of the same order of magnitude as the amplitude of magnetic dipole transition that evidenced a relatively stronger extent of the mirror symmetry violation at the Eu site in cesium europium sulfate, with respect to that in cesium europium sulfate hydrate.

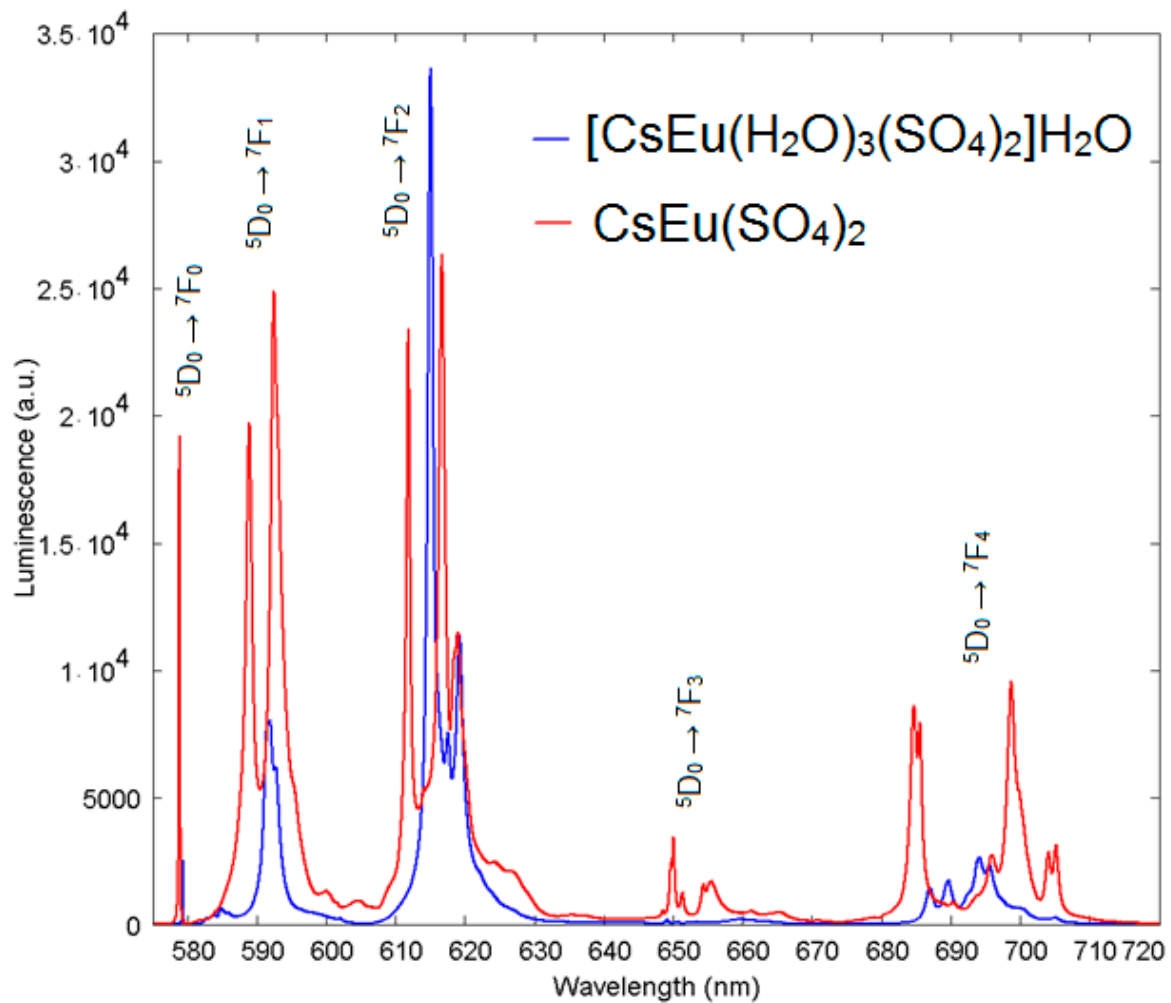


Figure 13. Emission spectra of $[\text{CsEu}(\text{H}_2\text{O})_3(\text{SO}_4)_2] \cdot \text{H}_2\text{O}$ (blue) and $\text{CsEu}(\text{SO}_4)_2$ (red).

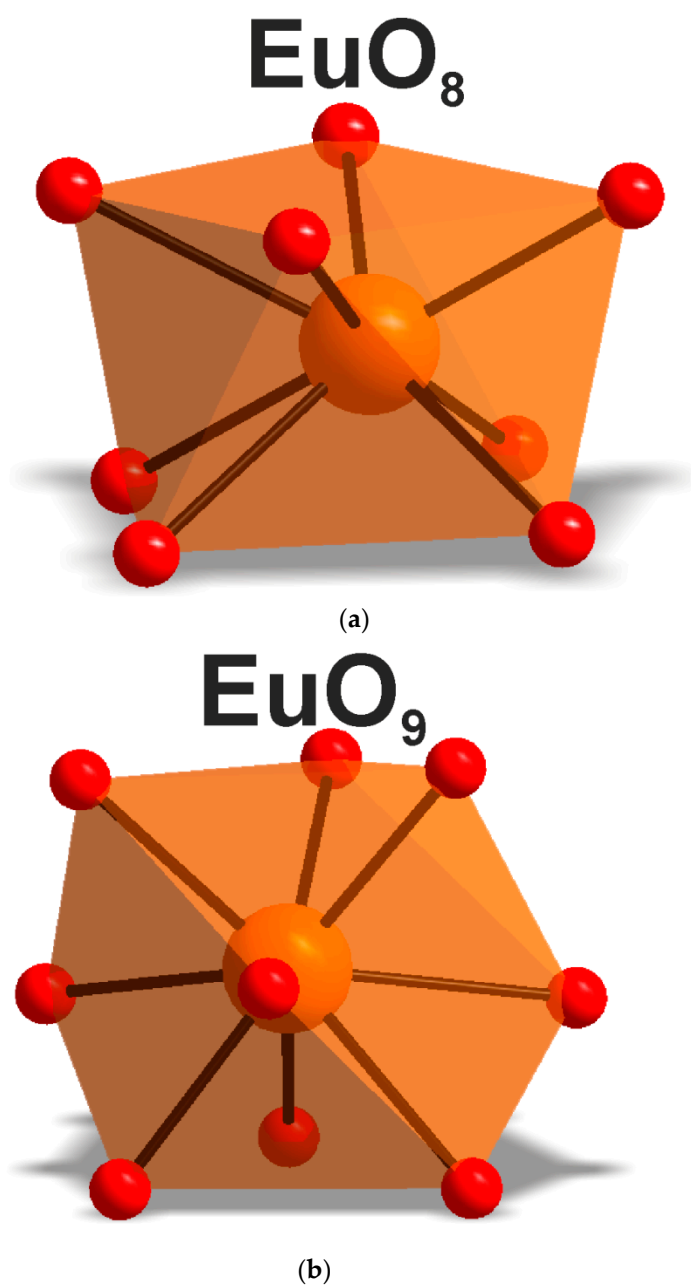


Figure 14. Local environment of the Eu^{3+} ion in (a) $\text{CsEu}(\text{SO}_4)_2$ and (b) $[\text{CsEu}(\text{H}_2\text{O})_3(\text{SO}_4)_2] \cdot \text{H}_2\text{O}$.

The extent of the chemical shift of the ultranarrow Eu line induced by the presence of H_2O molecules in the vicinity of the Eu site in cesium europium sulfate hydrate, with respect to cesium europium sulfate, is illustrated in more detail in Figure 15. The ultranarrow line position in cesium europium sulfate was at 578.8 nm, while in cesium europium sulfate hydrate it shifted to 579.3 nm.

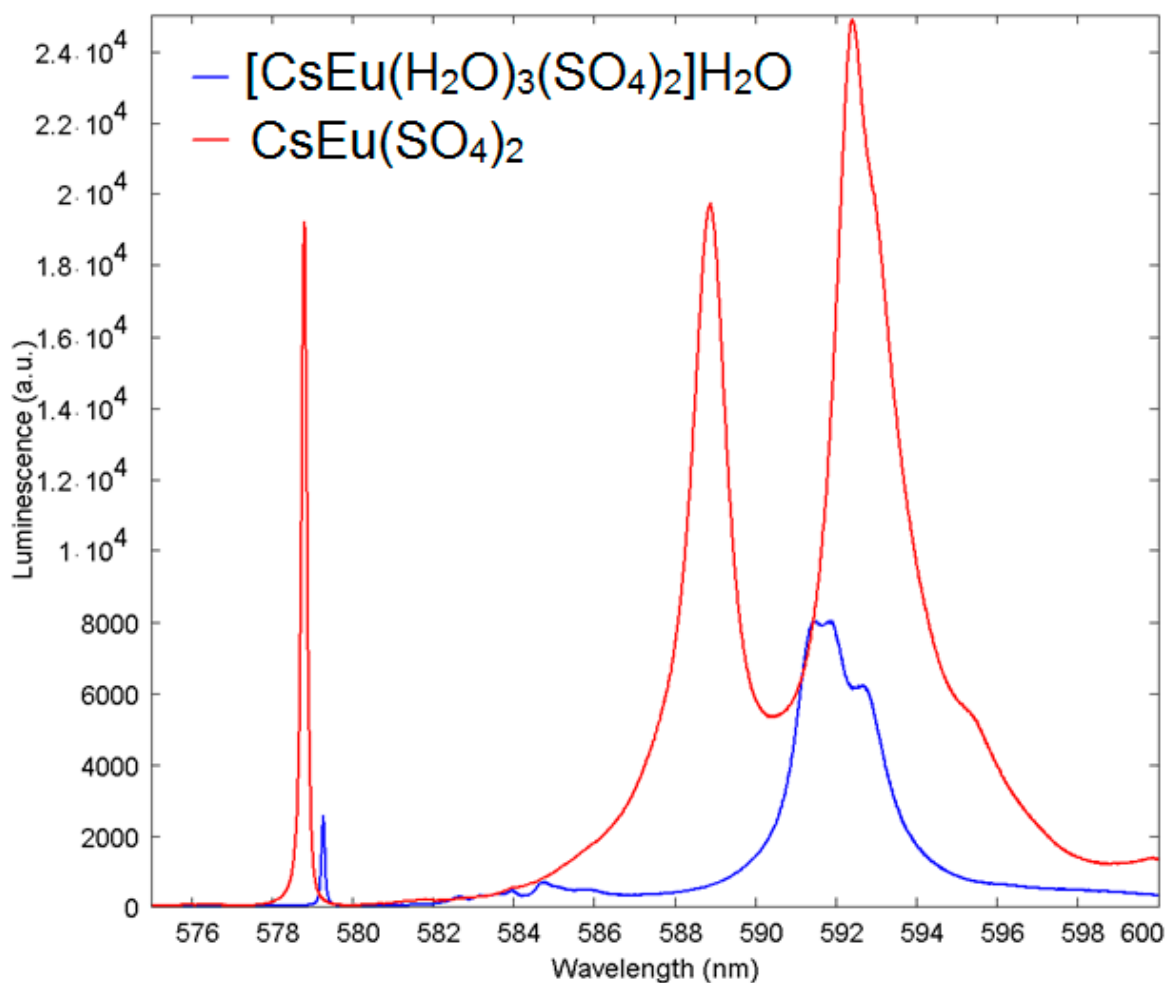


Figure 15. Luminescence spectra of Eu³⁺ in [CsEu(H₂O)₃(SO₄)₂].H₂O (blue) with respect to CsEu(SO₄)₂ (red) in the vicinity of the ultranarrow line ⁵D₀-⁷F₀ demonstrating the shift of ultranarrow line.

4. Conclusions

Thus, two new double sulfates [CsEu(H₂O)₃(SO₄)₂].H₂O and CsEu(SO₄)₂ were obtained and systematically investigated. The method of simple crystallization of their aqueous solution made it possible to obtain high quality single crystals of [CsEu(H₂O)₃(SO₄)₂].H₂O. The thermal dehydration provided the powder of anhydrous double sulfate CsEu(SO₄)₂ with a high stoichiometry, which is unattainable in a solid-phase reaction between simple sulfates. Both sulfates crystallized in a monoclinic system, but in different space groups, and it led to a significant difference in their vibrational, optical and luminescent properties. The band gap decreased on the transition from [CsEu(H₂O)₃(SO₄)₂].H₂O to CsEu(SO₄)₂. The thermochemical behavior of crystalline hydrate, which seemed illogical at first sight, was well explained by a detailed examination of the coordination of water molecules in the structure. A decisive aspect was found by the consideration of a system of hydrogen bonds, leading to an increased stability of one water molecule in the structure. The noticeable difference of the luminescence spectra between cesium europium sulfate and cesium europium sulfate hydrate was found and explained by the variation of the extent of local symmetry violation at the crystallographic sites occupied by Eu³⁺ ions, namely, the inversion symmetry and mirror symmetry. The chemical shift of the ⁵D₀ energy level in cesium europium sulfate hydrate, with respect to cesium europium sulfate, was associated with the presence of H₂O molecules in the vicinity of the Eu³⁺ ion.

Supplementary Materials: The following are available online at <https://www.mdpi.com/article/10.3390/cryst11091027/s1>, Table S1: Crystallographic data and main parameters of single crystal processing and refinement, Table S2: Coordinates of atoms and equivalent isotropic displacement parameters of Cs(Eu(H₂O)₃(SO₄)₂)·H₂O after single crystal refinement, Table S3: Main bond lengths of Cs(Eu(H₂O)₃(SO₄)₂)·H₂O, as obtained from single crystal refinement, Table S4: Fractional atomic coordinates and isotropic displacement parameters (Å²) of Cs(Eu(H₂O)₃(SO₄)₂)·(H₂O) after Rietveld refinement of powder pattern, Table S5: Main bond lengths (Å) of Cs(Eu(H₂O)₃(SO₄)₂)·(H₂O) obtained after Rietveld refinement of powder pattern, Table S6: Cell parameters of known compounds [A(Ln,Ac)(H₂O)₃(SO₄)₂]·H₂O, A = NH₄, Tl, Rb, Cs, Table S7: Fractional atomic coordinates and isotropic displacement parameters (Å²) of CsEu(SO₄)₂, Table S8: Main bond lengths (Å) of CsEu(SO₄)₂, Table S9: Raman and Infrared bands (cm⁻¹) observed in [CsEu(H₂O)₃(SO₄)₂]·H₂O and CsEu(SO₄)₂ and their assignments, related cif and checkcif files.

Author Contributions: Conceptualization, Y.G.D. and V.V.A.; methodology, I.A.R.; formal analysis, M.S.M. and A.S.O.; data curation, Y.G.D., A.S.K. and N.O.A.; writing—original draft preparation, Y.G.D., M.S.M., A.S.O. and A.S.A.; writing—review and editing, V.V.A.; supervision, O.V.A. All authors have read and agreed to the published version of the manuscript.

Funding: This work was partially supported by the Russian Foundation for Basic Research (grant 19-33-90258\19).

Conflicts of Interest: The authors declare no conflict of interest.

References

1. Davis, J.B.; Marshall, D.B.; Housley, R.M.; Morgan, P.E. Machinable ceramics containing rare-earth phosphates. *J. Am. Ceram. Soc.* **1998**, *81*, 2169–2175. [[CrossRef](#)]
2. Mortier, M.; Monteville, A.; Patriarche, G.; Mazé, G.; Auzel, F. New progresses in transparent rare-earth doped glass-ceramics. *Opt. Mater.* **2001**, *16*, 255–267. [[CrossRef](#)]
3. Tanabe, S.; Hayashi, H.; Hanada, T.; Onodera, N. Fluorescence properties of Er³⁺ ions in glass ceramics containing LaF₃ nanocrystals. *Opt. Mater.* **2002**, *19*, 343–349. [[CrossRef](#)]
4. Gonçalves, M.C.; Santos, L.; Almeida, R. Rare-earth-doped transparent glass ceramics. *Comptes Rendus Chim.* **2002**, *5*, 845–854. [[CrossRef](#)]
5. Mortier, M.; Bensalah, A.; Dantelle, G.; Patriarche, G.; Vivien, D. Rare-earth doped oxyfluoride glass-ceramics and fluoride ceramics: Synthesis and optical properties. *Opt. Mater.* **2007**, *29*, 1263–1270. [[CrossRef](#)]
6. Wang, J.; Liu, C.; Zhang, G.; Xie, J.; Han, J.; Zhao, X. Crystallization properties of magnesium aluminosilicate glass-ceramics with and without rare-earth oxides. *J. Non-Cryst. Solids* **2015**, *419*, 1–5. [[CrossRef](#)]
7. Wang, X.; Liu, Q.; Bu, Y.; Liu, C.-S.; Liu, T.; Yan, X. Optical temperature sensing of rare-earth ion doped phosphors. *RSC Adv.* **2015**, *5*, 86219–86236. [[CrossRef](#)]
8. Jianbei, Q.I.U.; Qing, J.I.A.O.; Dacheng, Z.H.O.U.; Zhengwen, Y. Recent progress on upconversion luminescence enhancement in rare-earth doped transparent glass-ceramics. *J. Rare Earths* **2016**, *34*, 341–367.
9. Atuchin, V.; Aleksandrovsky, A.; Molokeev, M.; Krylov, A.; Oreshonkov, A.; Zhou, D. Structural and spectroscopic properties of self-activated monoclinic molybdate BaSm₂(MoO₄)₄. *J. Alloy Compd.* **2017**, *729*, 843–849. [[CrossRef](#)]
10. Zou, Z.; Wu, T.; Lu, H.; Tu, Y.; Zhao, S.; Xie, S.; Han, F.; Xu, S. Structure, luminescence and temperature sensing in rare earth doped glass ceramics containing NaY(WO₄)₂ nanocrystals. *RSC Adv.* **2018**, *8*, 7679–7686. [[CrossRef](#)]
11. Laidler, J.; Battles, J.; Miller, W.; Ackerman, J.; Carls, E. Development of pyroprocessing technology. *Prog. Nucl. Energy* **1997**, *31*, 131–140. [[CrossRef](#)]
12. Preinfalk, C.; Morteani, G. *The Industrial Applications of Rare Earth Element: Lanthanides, Tantalum and Niobium*; Springer: Berlin/Heidelberg, Germany, 1989; pp. 359–370.
13. Jha, A.R. *Rare Earth Materials: Properties and Applications*; CRC Press: Boca Raton, FL, USA, 2014.
14. Ramana, C.V.; Vemuri, V.R.; Kaichev, V.; Kochubey, V.A.; Saraev, A.; Atuchin, V.V. X-ray photoelectron spectroscopy depth profiling of La₂O₃/Si thin films deposited by reactive magnetron sputtering. *ACS Appl. Mater. Interfaces* **2011**, *3*, 4370–4373. [[CrossRef](#)]
15. Xia, Z.; Zhang, Y.; Molokeev, M.S.; Atuchin, V.V. Structural and luminescence properties of yellow-emitting NaScSi₂O₆:Eu²⁺ phosphors: Eu²⁺ site preference analysis and generation of red emission by cooping Mn²⁺ for white-light-emitting diode applications. *J. Phys. Chem. C* **2013**, *117*, 20847–20854. [[CrossRef](#)]
16. Lim, C.S.; Aleksandrovsky, A.; Molokeev, M.; Oreshonkov, A.; Atuchin, V. Microwave sol-gel synthesis and upconversion photoluminescence properties of CaGd₂(WO₄)₄:Er³⁺/Yb³⁺ phosphors with incommensurately modulated structure. *J. Solid State Chem.* **2015**, *228*, 160–166. [[CrossRef](#)]
17. Ho, F.H.; Abdul-Rashid, S.H.; Ghazilla, R.A.R. Analytic hierarchy process-based analysis to determine the barriers to implementing a material efficiency strategy: Electrical and electronics' companies in the Malaysian context. *Sustainability* **2016**, *8*, 1035. [[CrossRef](#)]

18. Zhang, L.; Yang, F.; Zhong, S.-J. Whisker growth on SnAgCu-xPr solders in electronic packaging. *J. Mater. Sci. Mater. Electron.* **2016**, *27*, 5618–5621. [[CrossRef](#)]
19. Riba, J.-R.; Torres, C.L.; Romeral, L.; Garcia, A. Rare-earth-free propulsion motors for electric vehicles: A technology review. *Renew. Sustain. Energy Rev.* **2016**, *57*, 367–379. [[CrossRef](#)]
20. Xiao, Y.; Han, G.; Yue, J.; Hou, W.; Wu, J. Multifunctional rare-earth-doped tin oxide compact layers for improving performances of photovoltaic devices. *Adv. Mater. Interfaces* **2016**, *3*. [[CrossRef](#)]
21. Atuchin, V.V.; Subanakov, A.K.; Aleksandrovsky, A.S.; Bazarov, B.G.; Bazarova, J.G.; Dorzhieva, S.G.; Gavrilova, T.A.; Krylov, A.S.; Molokeyev, M.S.; Oreshonkov, A.S.; et al. Exploration of structural, thermal, vibrational and spectroscopic properties of new noncentrosymmetric double borate $\text{Rb}_3\text{NdB}_6\text{O}_{12}$. *Adv. Powder Technol.* **2017**, *28*, 1309–1315. [[CrossRef](#)]
22. Li, H.; Sheng, T.; Xue, Z.; Zhu, X.; Hu, S.; Wen, Y.; Fu, R.; Zhuo, C.; Wu, X. Synthesis, structure, characterization, and multifunctional properties of a family of rare earth organic frameworks. *CrystEngComm* **2017**, *19*, 2106–2112. [[CrossRef](#)]
23. Verma, S.; Amritphale, S.S.; Das, S. Multifunctional application of cytosine for the synthesis of hybrid homogenized nano-sized rare earth oxide (RE_2O_3) and rare earth oxycarbonate ($\text{RE}_2\text{O}_2\text{CO}_3$) (RE = Nd, Sm) advance material via microwave irradiation. *Prot. Met. Phys. Chem. Surf.* **2017**, *53*, 444–451. [[CrossRef](#)]
24. Ahmad, T.; Lone, I.H. Development of multifunctional lutetium ferrite nanoparticles: Structural characterization and properties. *Mater. Chem. Phys.* **2017**, *202*, 50–55. [[CrossRef](#)]
25. Ying, Z.; Jingqin, W.; Huiling, K. Study on electrical properties of AgSnO_2 contact materials doped with rare-earth La, Ce, and Y. *IEEE Trans. Compon. Packag. Manuf. Technol.* **2018**, *9*, 864–870. [[CrossRef](#)]
26. Azarapin, N.O.; Atuchin, V.V.; Maximov, N.G.; Aleksandrovsky, A.S.; Molokeyev, M.S.; Oreshonkov, A.S.; Shestakov, N.P.; Krylov, A.S.; Burkhanova, T.M.; Mukherjee, S.; et al. Synthesis, structure, melting and optical properties of three complex orthorhombic sulfides BaDyCuS_3 , BaHoCuS_3 and BaYbCuS_3 . *Mater. Res. Bull.* **2021**, *140*, 111314. [[CrossRef](#)]
27. Kaplyanskii, A.A.; Macfarlane, R. *Spectroscopy of Solids Containing Rare Earth Ions*; Elsevier: Amsterdam, The Netherlands, 1987.
28. Chatterjee, A.; Singh, A.K.; Jayaraman, A. Pressure-induced electronic collapse and structural changes in rare-earth monochalcogenides. *Phys. Rev. B* **1972**, *6*, 2285. [[CrossRef](#)]
29. Greenwood, N.; Earnshaw, A. *Chemistry of the Elements*; Elsevier: Amsterdam, The Netherlands, 1984.
30. Yu, D.; Tretyakov, L.I.; Martynenko, A.N.; Grigor'ev, A.; Tsivadze, Y. *Inorganic Chemistry: Chemistry of the Elements*; Students Book; Butterworth-Heinemann: Oxford, UK, 2001; pp. 131–204. (In Russian)
31. Cooper, B.R. Magnetic properties of rare earth metals. In *Solid State Physics*; Seitz, F., Turnbull, D., Ehrenreich, H., Eds.; Academic Press: Cambridge, MA, USA, 1968; Volume 21, pp. 393–490.
32. Wakeshima, M.; Nishimine, H.; Hinatsu, Y. Crystal structures and magnetic properties of rare earth tantalates RE_3TaO_7 (RE = rare earths). *J. Phys. Condens. Matter* **2004**, *16*, 4103–4120. [[CrossRef](#)]
33. Gupta, S.; Suresh, K.G. Review on magnetic and related properties of RTX compounds. *J. Alloys Compd.* **2015**, *618*, 562–606. [[CrossRef](#)]
34. Rahimi-Nasrabadi, M.; Behpour, M.; Sobhani-Nasab, A.; Hosseinpour-Mashkani, S.M. $\text{ZnFe}_{2-x}\text{La}_x\text{O}_4$ nanostructure: Synthesis, characterization, and its magnetic properties. *J. Mater. Sci. Mater. Electr.* **2015**, *26*, 9776–9781. [[CrossRef](#)]
35. Hinatsu, Y.; Doi, Y. Structures and magnetic properties of new fluorite-related quaternary rare earth oxides LnY_2TaO_7 and $\text{LaLn}_2\text{RuO}_7$ (Ln = rare earths). *J. Solid State Chem.* **2016**, *233*, 37–43. [[CrossRef](#)]
36. Nishiyama, A.; Doi, Y.; Hinatsu, Y. Magnetic interactions in rhenium-containing rare earth double perovskites $\text{Sr}_2\text{LnReO}_6$ (Ln = rare earths). *J. Solid State Chem.* **2017**, *248*, 134–141. [[CrossRef](#)]
37. Shi, P.; Xia, Z.; Molokeyev, M.S.; Atuchin, V.V. Crystal chemistry and luminescence properties of red-emitting $\text{CsGd}_{1-x}\text{Eu}_x(\text{MoO}_4)_2$ solid-solution phosphors. *Dalton Trans.* **2014**, *43*, 9669–9676. [[CrossRef](#)] [[PubMed](#)]
38. Ji, H.; Huang, Z.; Xia, Z.; Molokeyev, M.S.; Jiang, X.; Lin, Z.; Atuchin, V.V. Comparative investigations of the crystal structure and photoluminescence property of eulytite-type $\text{Ba}_3\text{Eu}(\text{PO}_4)_3$ and $\text{Sr}_3\text{Eu}(\text{PO}_4)_3$. *Dalton Trans.* **2015**, *44*, 7679–7686. [[CrossRef](#)]
39. Behrendt, M.; Mahlik, S.; Grinberg, M.; Stefańska, D.; Dereń, P.J. Influence of charge transfer state on Eu^{3+} luminescence in LaAlO_3 , by high pressure spectroscopy. *Opt. Mater.* **2017**, *63*, 158–166. [[CrossRef](#)]
40. Puchalska, M. High enhancement of Eu^{3+} luminescence in SrAl_4O_7 phosphor by means of charge compensation with Na^+ ions. *Opt. Mater.* **2017**, *72*, 452–458. [[CrossRef](#)]
41. Laishram, R.; Maitra, U. Bile salt-derived Eu^{3+} organogel and hydrogel: Water-enhanced luminescence of Eu^{3+} in a gel matrix. *ChemistrySelect* **2018**, *3*, 519–523. [[CrossRef](#)]
42. Li, S.; Wang, L.; Tang, D.; Cho, Y.; Liu, X.; Zhou, X.; Lu, L.; Zhang, L.; Takeda, T.; Hirotsaki, N.; et al. Achieving high quantum efficiency narrow-band β -Sialon: Eu^{2+} phosphors for high-brightness LCD backlights by reducing the Eu^{3+} luminescence killer. *Chem. Mater.* **2017**, *30*, 494–505. [[CrossRef](#)]
43. Van De Haar, M.A.; Werner, J.; Kratz, N.; Hilgerink, T.; Tachikirt, M.; Honold, J.; Krames, M. Increasing the effective absorption of Eu^{3+} -doped luminescent materials towards practical light emitting diodes for illumination applications. *Appl. Phys. Lett.* **2018**, *112*, 132101. [[CrossRef](#)]
44. Baur, F.; Jüstel, T. Uranyl sensitized Eu^{3+} luminescence in $\text{Ln}(\text{UO}_2)_3(\text{PO}_4)_2\text{O}(\text{OH})\cdot 6\text{H}_2\text{O}$ phosphors (Ln = Y, Eu, La) for warm-white light emitting diodes. *J. Lumin.* **2018**, *196*, 431–436. [[CrossRef](#)]

45. Shi, X.; Wang, Z.; Takei, T.; Wang, X.; Zhu, Q.; Li, X.; Kim, B.-N.; Sun, X.; Li, J.-G. Selective crystallization of four tungstates ($\text{La}_2\text{W}_3\text{O}_{12}$, $\text{La}_2\text{W}_2\text{O}_9$, $\text{La}_{14}\text{W}_8\text{O}_{45}$, and $\text{La}_6\text{W}_2\text{O}_{15}$) via hydrothermal reaction and comparative study of Eu^{3+} luminescence. *Inorg. Chem.* **2018**, *57*, 6632–6640. [[CrossRef](#)]
46. Li, C.; Fan, X.; Jiang, P.; Jin, X. Delamination-indicating of atmosphere-plasma-sprayed thermal barrier coating system using Eu^{3+} luminescence mapping. *Mater. Lett.* **2018**, *222*, 41–44. [[CrossRef](#)]
47. Paama, L.; Pitkänen, I.; Valkonen, J.; Pärnoja, E.; Kola, H.; Perämäki, P. Thermal and spectroscopic investigation of europium and samarium sulphates hydrates by TG-FTIR and ICP-MS techniques. *Talanta* **2005**, *67*, 897–902. [[CrossRef](#)] [[PubMed](#)]
48. Xu, Y.; Ding, S.; Zheng, X. Hydrothermal synthesis, crystal structure and properties of 2-D and 3-D lanthanide sulfates. *J. Solid State Chem.* **2007**, *180*, 2020–2025. [[CrossRef](#)]
49. Choi, M.-H.; Kim, M.-K.; Jo, V.; Lee, D.-W.; Shim, I.-W.; Ok, K.M. Hydrothermal syntheses, structures, and characterizations of two lanthanide sulfate hydrates materials, $\text{La}_2(\text{SO}_4)_3 \cdot \text{H}_2\text{O}$ and $\text{Eu}_2(\text{SO}_4)_3 \cdot 4\text{H}_2\text{O}$. *Bull. Korean Chem. Soc.* **2010**, *31*, 1077–1080. [[CrossRef](#)]
50. Zhang, X.; Ma, Y.; Zhao, H.; Jiang, C.; Sun, Y.; Xu, Y. Synthesis, characterization and very strong luminescence of a new 3D europium sulfate $\text{Eu}_2(\text{H}_2\text{O})_4(\text{SO}_4)_3$. *J. Struct. Chem.* **2011**, *52*, 954–958. [[CrossRef](#)]
51. Wang, X.J.; Molokeev, M.S.; Zhu, Q.; Li, J.G. Controlled hydrothermal crystallization of anhydrous $\text{Ln}_2(\text{OH})_4\text{SO}_4$ (Ln = Eu-Lu, Y) as a new family of layered rare earth metal hydroxides. *Chem. Eur. J.* **2017**, *23*, 16034–16043. [[CrossRef](#)] [[PubMed](#)]
52. Atuchin, V.V.; Subanakov, A.K.; Aleksandrovsky, A.S.; Bazarov, B.G.; Bazarova, J.G.; Gavrilova, T.A.; Krulov, A.S.; Molokeev, M.S.; Oreshonkov, A.S.; Stefanovich, S.Y. Structural and spectroscopic properties of noncentrosymmetric self-activated borate $\text{Rb}_3\text{EuB}_6\text{O}_{12}$ with B_5O_{10} units. *Mater. Des.* **2018**, *140*, 488–494. [[CrossRef](#)]
53. Denisenko, Y.G.; Atuchin, V.V.; Molokeev, M.S.; Aleksandrovsky, A.S.; Krylov, A.S.; Oreshonkov, A.S.; Volkova, S.S.; Andreev, O.V. Structure, thermal stability, and spectroscopic properties of triclinic double sulfate $\text{AgEu}(\text{SO}_4)_2$ with isolated SO_4 groups. *Inorg. Chem.* **2018**, *57*, 13279–13288. [[CrossRef](#)]
54. Lal, H.B.; Lundgren, L. Magnetic susceptibility, electrical conductivity and dielectric constant of $\text{Eu}_2(\text{WO}_4)_3$ single crystals. *J. Phys. Soc. Jpn.* **1976**, *41*, 1216–1223. [[CrossRef](#)]
55. Lal, H.; Dar, N. Magnetic susceptibility of $\text{Eu}_2(\text{WO}_4)_3$ single crystals. *Phys. B + C* **1976**, *84*, 254–258. [[CrossRef](#)]
56. Huang, Q.; Xu, J.Z.; Li, W. Preparation of tetragonal defect scheelite-type $\text{RE}_2(\text{MoO}_4)_3$ (RE = La to Ho) by precipitation method. *Solid State Ion.* **1989**, *32*, 244–249. [[CrossRef](#)]
57. Imanaka, N.; Hiraiwa, M.; Tamura, S.; Adachi, G. A new realization route of $\text{Al}_2(\text{WO}_4)_4\text{-Ln}_2(\text{WO}_4)_3$ (Ln = Lu, Eu) solid solution single crystals by electrochemical ion doping. *Electrochem. Solid-State Lett.* **1999**, *2*, 570–571. [[CrossRef](#)]
58. Dmitriev, V.; Sinitsyn, V.; Dilanian, R.; Machon, D.; Kuznetsov, A.; Ponyatovsky, E.; Lucazeau, G.; Weber, H.P. In situ pressure-induced solid-state amorphization in $\text{Sm}_2(\text{MoO}_4)_3$, $\text{Eu}_2(\text{MoO}_4)_3$ and $\text{Gd}_2(\text{MoO}_4)_3$ crystals: Chemical decomposition scenario. *J. Phys. Chem. Solids* **2003**, *64*, 307–312. [[CrossRef](#)]
59. Kodaira, C.; Brito, H.; Malta, O.; Serra, O. Luminescence and energy transfer of the europium (III) tungstate obtained via the Pechini method. *J. Lumin.* **2003**, *101*, 11–21. [[CrossRef](#)]
60. Machon, D.; Dmitriev, V.P.; Sinitsyn, V.V.; Lucazeau, G. $\text{Eu}_2(\text{MoO}_4)_3$ single crystal at high pressure: Structural phase transitions and amorphization probed by fluorescence spectroscopy. *Phys. Rev. B* **2004**, *70*, 094117. [[CrossRef](#)]
61. Shmyt'ko, I.M.; Kudrenko, E.A.; Sinitsyn, V.V.; Red'kin, B.S.; Ponyatovsky, E.G. Features of the pressure-induced phase transitions in $\text{Eu}_2(\text{MoO}_4)_3$ single crystals. *J. Exp. Theor. Phys. Lett.* **2005**, *82*, 409–412. [[CrossRef](#)]
62. Park, K.-C.; Ahn, H.-C.; Nguyen, H.-D.; Jang, H.-Y.; Mho, S.-I. Optical properties of $\text{Eu}_2(\text{WO}_4)_3$ and $\text{Tb}_2(\text{WO}_4)_3$ and of CaWO_4 doped with Eu^{3+} or Tb^{3+} —Revisited. *J. Korean Phys. Soc.* **2008**, *53*, 2220–2223. [[CrossRef](#)]
63. Martinez-Garcia, J.; Arakcheeva, A.; Pattison, P.; Morozov, V.; Chapuis, G. Validating the model of a (3 + 1)-dimensional incommensurately modulated structure as generator of a family of compounds for the $\text{Eu}_2(\text{MoO}_4)_3$ scheelite structure. *Philos. Mag. Lett.* **2009**, *89*, 257–266. [[CrossRef](#)]
64. Wang, Y.; Honma, T.; Doi, Y.; Hinatsu, Y.; Komatsu, T. Magnetism of β' - $\text{Gd}_2(\text{MoO}_4)_3$ and photo-luminescence of β' - $\text{Eu}_2(\text{MoO}_4)_3$ crystallized in rare-earth molybdenum borate glasses. *J. Ceram. Soc. Jpn.* **2013**, *121*, 230–235. [[CrossRef](#)]
65. Atuchin, V.V.; Aleksandrovsky, A.; Chimitova, O.D.; Gavrilova, T.A.; Krylov, A.; Molokeev, M.; Oreshonkov, A.S.; Bazarov, B.G.; Bazarova, J.G. Synthesis and spectroscopic properties of monoclinic α - $\text{Eu}_2(\text{MoO}_4)_3$. *J. Phys. Chem. C* **2014**, *118*, 15404–15411. [[CrossRef](#)]
66. Lahoz, F.; Sabalisk, N.P.; Cerdeiras, E.; Mestres, L. Nano-to millisecond lifetime luminescence properties in $\text{Ln}_2(\text{WO}_4)_3$ (Ln = La, Ho, Tm and Eu) microcrystalline powders with different crystal structures. *J. Alloys Compd.* **2015**, *649*, 1253–1259. [[CrossRef](#)]
67. Denisenko, Y.G.; Aleksandrovsky, A.; Atuchin, V.; Krylov, A.; Molokeev, M.; Oreshonkov, A.; Shestakov, N. Exploration of structural, thermal and spectroscopic properties of self-activated sulfate $\text{Eu}_2(\text{SO}_4)_3$ with isolated SO_4 groups. *J. Ind. Eng. Chem.* **2018**, *68*, 109–116. [[CrossRef](#)]
68. Sirotinkin, S.P.; Efremov, V.A.; Kovba, L.M.; Pokrovskii, A.N. Crystal structure of lithium-europium double sulfate. *Kristallografiya* **1977**, *22*, 966–970.
69. Iyer, P.N.; Kulkarni, N.K. Preparation and characterization of $\text{TIMIII}(\text{SO}_4)_2 \cdot 4\text{H}_2\text{O}$ (M (III) \equiv Pu, Sm to Dy). *J. Alloys Compd.* **1995**, *217*, 253–257. [[CrossRef](#)]
70. Iyer, P.N.; Mudher, K.D.S.; Kulkarni, N.K. Preparation and characterisation of $\text{TILn}(\text{SO}_4)_2 \cdot \text{H}_2\text{O}$ (Ln = Sm to Lu, Y). *J. Alloys Compd.* **1997**, *252*, 71–75. [[CrossRef](#)]

71. Kazmierczak, K.; Höpfe, H.A. Syntheses, crystal structures and vibrational spectra of $\text{KLn}(\text{SO}_4)_2 \cdot \text{H}_2\text{O}$ ($\text{Ln} = \text{La}, \text{Nd}, \text{Sm}, \text{Eu}, \text{Gd}, \text{Dy}$). *J. Solid State Chem.* **2010**, *183*, 2087–2094. [CrossRef]
72. Atuchin, V.V.; Aleksandrovsky, A.S.; Bazarov, B.G.; Bazarova, J.G.; Chimitova, O.D.; Denisenko, Y.G.; Gavrilova, T.A.; Krylov, A.S.; Maximovskiy, E.A.; Molochev, M.S.; et al. Exploration of structural, vibrational and spectroscopic properties of self-activated orthorhombic double molybdate $\text{RbEu}(\text{MoO}_4)_2$ with isolated MoO_4 units. *J. Alloys Compd.* **2019**, *785*, 692–697. [CrossRef]
73. Yamamoto, H.; Seki, S.; Ishiba, T. The Eu site symmetry in $\text{AEu}(\text{MoO}_4)_2$ ($\text{A} = \text{Cs}$ or Rb) generating saturated red luminescence. *J. Solid State Chem.* **1991**, *94*, 396–403. [CrossRef]
74. Wang, Z.; Liang, H.; Gong, M.; Su, Q. The red phosphor $\text{NaEu}(\text{MoO}_4)_2$ prepared by the combustion method. *Mater. Lett.* **2008**, *62*, 619–622. [CrossRef]
75. Guo, C.; Wang, S.; Chen, T.; Luan, L.; Xu, Y. Preparation of phosphors $\text{AEu}(\text{MoO}_4)_2$ ($\text{A} = \text{Li}, \text{Na}, \text{K}$ and Ag) by sol-gel method. *Appl. Phys. A* **2009**, *94*, 365–371. [CrossRef]
76. Huang, J.; Xu, J.; Luo, H.; Yu, X.; Li, Y. Effect of alkali-metal ions on the local structure and luminescence for double tungstate compounds $\text{AEu}(\text{WO}_4)_2$ ($\text{A} = \text{Li}, \text{Na}, \text{K}$). *Inorg. Chem.* **2011**, *50*, 11487–11492. [CrossRef]
77. Perles, J.; Fortes-Revilla, C.; Gutierrez-Puebla, E.; Iglesias, M.; Monge, M.A.; Ruiz-Valero, A.C.; Snejko, N. Synthesis, structure, and catalytic properties of rare-earth ternary sulfates. *Chem. Mater.* **2005**, *17*, 2701–2706. [CrossRef]
78. Deng, Z.; Bai, F.; Xing, Y.; Xing, N.; Xu, L. Reaction in situ found in the synthesis of a series of lanthanide sulfate complexes and investigation on their structure, spectra and catalytic activity. *Open J. Inorg. Chem.* **2013**, *3*, 76–99. [CrossRef]
79. Denisenko, Y.G.; Sedykh, A.E.; Molochev, M.S.; Oreshonkov, A.S.; Aleksandrovsky, A.S.; Krylov, A.S.; Nikolay, A.; Khritokhin, E.; Sal'nikova, I.; Andreev, O.V.; et al. Crystal and electronic structure, thermochemical and photophysical properties of europium-silver sulfate monohydrate $\text{AgEu}(\text{SO}_4)_2 \cdot \text{H}_2\text{O}$. *J. Solid State Chem.* **2021**, *294*, 121898. [CrossRef]
80. Jasty, S.; Malhotra, V.M.; Robinson, P.D. Effect of the lanthanide ion on the structure and low-temperature phase transitions in $\text{RbL}(\text{SO}_4)_2 \cdot 4\text{H}_2\text{O}$ ($\text{L} \equiv \text{La} - \text{Er}$) crystals. *J. Phys. Condens. Matter* **1992**, *4*, 4769–4778. [CrossRef]
81. Eriksson, B.; Larsson, L.O.; Niinisto, L.; Skoglund, U. Crystal structure of ammonium samarium sulfate tetrahydrate. *Inorg. Chem.* **1974**, *13*, 290–295. [CrossRef]
82. Chadha, A.; Sampath, S.; Chackraburty, D. X-ray powder diffraction and thermal studies on some uranium (III) compounds. *Inorg. Chim. Acta* **1980**, *42*, 163–167. [CrossRef]
83. Safianov, I.N.; Kuz'min, E.A.; Iskhakova, L.D.; Ilyukhin, V.V.; Belov, N.V. Crystal structure of double Cs,La-sulphate, $\text{Cs}_2\text{SO}_4 \cdot \text{La}_2(\text{SO}_4)_3 \cdot 8\text{H}_2\text{O}$. *Dokl. Akad. Nauk. SSSR* **1975**, *220*, 346–348.
84. Bukovec, P.; Golic, L. The salts and double salts of rare earths. Crystal structure of cesium bi-sulfate tri-aquopraseodimate (III) monohydrate. *Vestn. Slov. Kem. Drus.* **1975**, *22*, 19–25.
85. Bukovec, N.; Golic, L.; Siftar, J. The salts and double salts of rare earths. Structural study of dehydration differences between $\text{Cs}[\text{Pr}(\text{SO}_4)_2(\text{H}_2\text{O})_3] \cdot \text{H}_2\text{O}$ and $\text{Cs}[\text{Lu}(\text{SO}_4)_2(\text{H}_2\text{O})_3] \cdot \text{H}_2\text{O}$. *Vestn. Slov. Kem. Drus.* **1979**, *26*, 377–385.
86. Boujelben, M.; Toumi, M.; Mhiri, T. $\text{NH}_4\text{Ce}(\text{SO}_4)_2 \cdot 4\text{H}_2\text{O}$. *Acta Cryst. E* **2007**, *63*, i144–i145. [CrossRef]
87. Atuchin, V.V.; Gavrilova, T.A.; Kuratieva, N.V.; Okotrub, K.A.; Pervukhina, N.V.; Surovtsev, N.V. Sublimation growth and vibrational microspectrometry of $\alpha\text{-MoO}_3$ single crystals. *J. Cryst. Growth* **2011**, *318*, 987–990. [CrossRef]
88. Alekseev, E.V.; Felbinger, O.; Wu, S.; Malcherek, T.; Depmeier, W.; Modolo, G.; Gesing, T.M.; Krivovichev, S.V.; Suleimanov, E.V.; Gavrilova, T.A.; et al. $\text{K}[\text{AsW}_2\text{O}_9]$, the first member of the arsenate tungsten bronze family: Synthesis, structure, spectroscopic and non-linear optical properties. *J. Solid State Chem.* **2013**, *204*, 59–63. [CrossRef]
89. Kokh, K.; Atuchin, V.; Gavrilova, T.; Kuratieva, N.; Pervukhina, N.; Surovtsev, N. Microstructural and vibrational properties of PVT grown Sb_2Te_3 crystals. *Solid State Commun.* **2014**, *177*, 16–19. [CrossRef]
90. Troitskaia, I.B.; Gavrilova, T.A.; Gromilov, S.A.; Sheglov, D.V.; Atuchin, V.V.; Vemuri, R.S.; Ramana, C.V. Growth and structural properties of $\alpha\text{-MoO}_3$ (010) microplates with atomically flat surface. *Mater. Sci. Eng. B* **2010**, *174*, 159–163. [CrossRef]
91. Denisenko, Y.; Khritokhin, N.; Andreev, O.; Basova, S.; Sal'nikova, E.; Polkovnikov, A. Thermal decomposition of europium sulfates $\text{Eu}_2(\text{SO}_4)_3 \cdot 8\text{H}_2\text{O}$ and EuSO_4 . *J. Solid State Chem.* **2017**, *255*, 219–224. [CrossRef]
92. Sheldrick, G.M. Crystal structure refinement with SHELXL. *Acta Crystallogr. Sect. C Struct. Chem.* **2015**, *71*, 3–8. [CrossRef]
93. Spek, A.L. PLATON—A Multipurpose Crystallographic Tool. Ph.D. Thesis, Utrecht University, Utrecht, The Netherlands, 2008.
94. Brandenburg, K.; Berndt, M. DIAMOND—Visual Crystal Structure Information System CRYSTAL IMPACT. *J. Appl. Crystallogr.* **1999**, *32*, 1028–1029.
95. Bruker. TOPAS V4: General Profile and Structure Analysis Software for Powder Diffraction Data—User's Manual. 2008. Available online: <http://algol.fis.uc.pt/jap/TOPAS%204-2%20Users%20Manual.pdf> (accessed on 8 August 2021).
96. Sarukhanyan, N.L.; Iskhakova, L.D.; Trunov, V.K. Crystal structure of $\text{RbEu}(\text{SO}_4)_2$. *Kristallografiya* **1983**, *28*, 452–456.
97. Clark, S.; Segall, M.D.; Pickard, C.J.; Hasnip, P.J.; Probert, M.I.J.; Refson, K.; Payne, M.C. First principles methods using CASTEP. *Cryst. Mater.* **2005**, *220*, 567–570. [CrossRef]
98. Perdew, J.P.; Zunger, A. Self-interaction correction to density-functional approximations for many-electron systems. *Phys. Rev. B* **1981**, *23*, 5048–5079. [CrossRef]
99. Ceperley, D.; Alder, B. Ground state of the electron gas by a stochastic method. *Phys. Rev. Lett.* **1980**. [CrossRef]
100. Nakamoto, K. *Infrared and Raman Spectra of Inorganic and Coordination Compounds*, 6th ed.; Wiley and Sons: New York, NY, USA, 2009.
101. Tauc, J. Optical properties and electronic structure of amorphous Ge and Si. *Mater. Res. Bull.* **1968**, *3*, 37–46. [CrossRef]

-
102. Hinuma, Y.; Pizzi, G.; Kumagai, Y.; Oba, F.; Tanaka, I. Band structure diagram paths based on crystallography. *Comput. Mater. Sci.* **2017**, *128*, 140–184. [[CrossRef](#)]
 103. Kolesnikov, I.; Kolokolov, D.; Kurochkin, M.; Voznesenskiy, M.; Osmolowsky, M.; Lähderanta, E.; Osmolovskaya, O. Morphology and doping concentration effect on the luminescence properties of SnO₂:Eu³⁺ nanoparticles. *J. Alloy Compd.* **2020**, *822*, 153640. [[CrossRef](#)]